Ruthenium(II) complexes with phosphonate-substituted phenanthroline ligands: synthesis, characterization and use in organic photocatalysis

Gleb V. Morozkov, Anton S Abel, Mikhail A. Filatov, Sergei E Nefedov, Vitaly A. Roznyatovsky, Andrey V. Cheprakov, Alexander Yu. Mitrofanov, Ilia S. Ziankou, Alexei D. Averin, Irina P. Beletskaya, et al.

Ruthenium(II) complexes with phosphonate-substituted phenanthroline ligands: synthesis, characterization and use in organic photocatalysis

Gleb V. Morozkov,[a] Anton S. Abel,*[a] Mikhail A. Filatov,[b] Sergei E. Nefedov,[c] Vitaly A. Roznyatovsky,[a] Andrey V. Cheprakov,[a] Alexander Yu. Mitrofanov,[a,d] Ilia S. Ziankou,[a,d] Alexei D. Averin,[a] Irina P. Beletskaya,[a] Julien Michalak,[d] Christophe Bucher,*[e] Laurent Bonneviot,[e] Alla Bessmertnykh-Lemeune*[d,e]

[a] *Lomonosov Moscow State University, Department of Chemistry, 1-3, Leninskie Gory, Moscow, 119991, Russia*

[b] *School of Chemical and Pharmaceutical Sciences, Technological University Dublin, City Campus, Grangegorman, Dublin 7, Ireland*

[c] *N.S. Kurnakov Institute of General and Inorganic Chemistry RAS, 119991, Leninsky pr., 31, Moscow, Russian Federation*

[d] *Institut de Chimie Moléculaire de l'Université de Bourgogne, UMR CNRS 6302, Université Bourgogne Franche-Comté, 9 Avenue Alain Savary, 21078 Dijon, France*

[e] *ENS de Lyon, UMR 5182, CNRS, Laboratoire de Chimie, 69342 Lyon, France*

ABSTRACT: Ru(II) complexes with polypyridyl ligands play a central role in the development of photocatalytic organic reactions. This work is aimed at the structural modification of such complexes to increase their photocatalytic efficiency and adapt them for the preparation of reusable photocatalytic systems. Nine $[Ru(phen)(bpy)_2]^{2+}$-type complexes (bpy = 2,2′-bipyridine, phen = 1,10-phenanthroline) (**Ru-Pcat**) bearing the $P(O)(OEt)_2$ substituent attached to the phen core directly or through a 1,4-phenylene linker were synthesized and characterized by spectroscopic and electrochemical techniques. Coordination mode of phen ligands was confirmed by single crystal X-ray analysis. The (spectro)electrochemical data show that the first electron transfer in **Ru-Pcat** is taking place on the phen ligand. The emission maxima and quantum yields are strongly affected by the substitution pattern, reaching the far-red region (697 nm) for **Ru-3,8P$_2$**. The singlet oxygen quantum yields of **Ru-Pcat** were evaluated using chemical trapping method. Finally, photocatalytic performance of **Ru-Pcat** in the oxidation of sulfides by molecular oxygen was investigated. Both dialkyl and alkyl aryl sulfides were quantitatively transformed into sulfoxides under irradiation with blue LED in the acetonitrile–water mixture (10:1) using a low loading of 0.005–0.05 mol% of Ru(II) photocatalysts. To rationalize the effect of phosphonate substituents on the photocatalytic efficiency, comparative kinetic studies of 1) 4-nitrothioanisole oxidation proceeding predominantly *via* electron transfer pathway and 2)

oxidation of dibutyl sulfide wherein singlet oxygen serves as an oxidant have been performed. It was demonstrated that complexes with $P(O)(OEt)_2$ substituent in positions 4 and 7 outperform the benchmark photocatalyst **Ru-(bpy)$_3$** and the parent complex **Ru-phen** in the reactions proceeding through electron transfer (reductive quenching photocatalytic cycle). The TON in the oxidation of 4-methoxythioanisole was found to be as high as 1,000,000 that is, to our knowledge, the highest among previously reported photocatalysts. In contrast, upon separating the $P(O)(OEt)_2$ group and the phen core by 1,4-phenylene linker, singlet oxygen quantum yields significantly increase that favors reactions proceeding through the energy transfer (the oxidation of dibutyl sulfide in our case). Thus, both series of Ru(II) complexes prepared in this work are promising for the improvement of known photocatalytic reactions and development of new transformations.

INTRODUCTION

Visible light-active Ru(II) and Ir(III) complexes with chelating ligands containing pyridyl residues (VATMPY complexes) such as 2,2´-bipyridine (bpy), 1,10-phenanthroline (phen) and 2,2´,6´,2´´-terpyridine have been intensively studied for more than a half of century due to their relevance to molecular electronics, host-guest modeling, functional supramolecular systems and labeling of biomolecules, electro- and photocatalysis.[1-6] They also found applications in organic synthesis as photosensitizers for the oxidation of unsaturated compounds, phosphines and sulfides by molecular oxygen.[7] During the last decade impressive progress has been achieved in their application as catalysts in the visible light-driven photoredox catalytic reactions.[8-10] The excited states of Ru(II) or Ir(III) complexes with bpy ligands have both the oxidizing (Ru(III) or Ir(IV)) and reducing ($bpy^{\bullet-}$) sites[11] and can mediate a wide range of organic reactions proceeding through both reductive or oxidative quenching photocatalytic cycles.

Among many light-active organic compounds and metal complexes, which were successfully used as photoredox catalysts, Ru(II) and Ir(III) complexes are attracting particular interest due to their high light absorptivity, high reduction and oxidation potentials and exceptional photostability. Moreover, redox and spectroscopic properties of these complexes can be fine-tuned by the introduction of substituents at the periphery of polypyridyl ligands.[12] The catalyst screening has been recognized as an efficient tool in the photoreactions optimization, but the number of Ru(II) and Ir(III) complexes which have been investigated is rather limited and $[Ru(bpy)_3]^{2+}$ is still a benchmark photocatalyst among Ru(II)

complexes.[10] This is in part due to laborious synthesis of these complexes and rather obscure understanding of Structure–Activity Relationships in photocatalytic reactions.

Some relevant information on the substituent effect in photocatalytic reactions can be gathered from data obtained in more mature fields where Ru(II) and Ir(III) complexes were applied, e. g., in electron transfer processes, light harvesting, binding to DNA and water splitting.[13-18] For instance, an investigation of electron transfer reactions between ruthenium(II) complexes with bpy ligands and triethylamine (NEt_3) showed that the back electron transfer can be retarded by introducing hydrophobic substituents in the pyridine ring that favors chemical transformation of intermediates arising after the initial electron transfer step.[19] This observation led to one of the early example of photoredox catalyzed reactions, i. e., the oxidative hydrolysis of NEt_3 to acetaldehyde,[19] which led to a conclusion that the efficiency of photoredox catalysts is governed not only by electronic properties of substituents but also by their hydrophobicity and steric effects.[19,20] In recent years, the development of Structure–Activity Relationships for VATMPY complexes attracted some attention.[21-23] However, despite the increasing amount of data on photophysical and redox properties of such compounds, the development of reliable guidelines for designing complexes, which meet specific performance criteria remains a challenge.[24]

Our work is focused on the optimization of Ru(II) photocatalysts efficiency. Although only a single polypyridyl ligand is required to acquire MLCT transitions in these complexes,[14] the replacement of one bpy ligand in the coordination shell of ruthenium atom by another specific chelator can have detrimental effect on photophysical properties and reactivity.[25] Taking this into account, we explored the functionalization of polypyridyl ligands as a way to increase catalytic efficiency of Ru(II) photocatalysts. In this work, we synthesized two series of mixed ligand $[Ru(phen)(bpy)_2]^{2+}$-type complexes (**Ru-Pcat**), in which the phen ligand is functionalized by diethoxyphosphoryl group ($P(O)(OEt)_2$) (Figure 1) and investigated their photocatalytic properties in the photooxidation of sulfides to sulfoxides by molecular oxygen. In the first series (**Ru-P**) the phosphorous substituent is directly bonded to the phen core, while in the second series (**Ru-PPh**), these fragments are separated by a 1,4-phenylene spacer, which allows for a systematic tuning of photophysical and redox properties of the studied complexes. 1,10-Phenanthrolines bearing a phosphonate substituent in position 2 were excluded from these investigations because bleaching of Ru(II) complexes which involves the photoinduced ligand dissociation may be accelerated in these complexes due to steric strain around the Ru(II) center.

The hydrophilic and strongly electron-withdrawing $P(O)(OEt)_2$ group could offer several benefits relevant to photocatalytic applications such as increasing solubility of photocatalysts in solvents with medium polarity and fine tuning of their redox potentials. Moreover, diesters of phosphonic acids can be easily transformed into phosphonic acids or their mono esters, both useful for further development of water-soluble photocatalysts. Finally, the phosphonate substituent is a well-known anchoring group for grafting organic compounds and metal complexes onto inorganic supports such as titanium or zirconium oxides.[26,27] Heterogeneous photocatalysts prepared according to this strategy could be made reusable that is an important goal in sustainable organic synthesis involving precious metal complexes.

Ru(II) complexes bearing phosphonate-substituted bpy ligands were prepared for photovoltaic applications[28-35] and recently used in organic photocatalysis.[36-38] We were interested to attach this group to the phen ligand, which is known for inertness in the ligand exchange reactions. Coordination lability of ligands is a serious drawback often observed in photocatalytic reactions to account for non-radiative relaxation of excited photocatalysts and photobleaching.[39]

Our initial efforts in the studies of phosphonate-substituted Ru(II) complexes involved their synthesis, characterization and application in the oxidation of sulfides by molecular oxygen. By comparing these complexes and common Ru(II) photocatalysts such as tris(2,2'-bipyridine)ruthenium(II) hexafluorophosphate (**Ru-(bpy)$_3$**), bis(2,2′-bipyridine)(1,10-phenanthroline)ruthenium(II) hexafluorophosphate (**Ru-phen)** and tris(1,10-phenanthroline)ruthenium(II) hexafluorophosphate (**Ru-(phen)$_3$**), we gained insight into the influence of the substitution pattern on photocatalytic properties. The results obtained in this work emphasize the potential utility of 4-substituted and 4,7-disubstituted complexes as photocatalysts in reactions involving either electron transfer or energy transfer. Notably, an unprecedented TON of almost 1,000,000 was achieved in the photooxidation of 4-methoxythioanisole to sulfoxide using 4,7-di-phosphonate-substituted complex **Ru-4,7P$_2$** as a photocatalyst.

When our work was in progress,[40] the synthesis of **Ru-5P** and its use in water splitting was reported.[41]

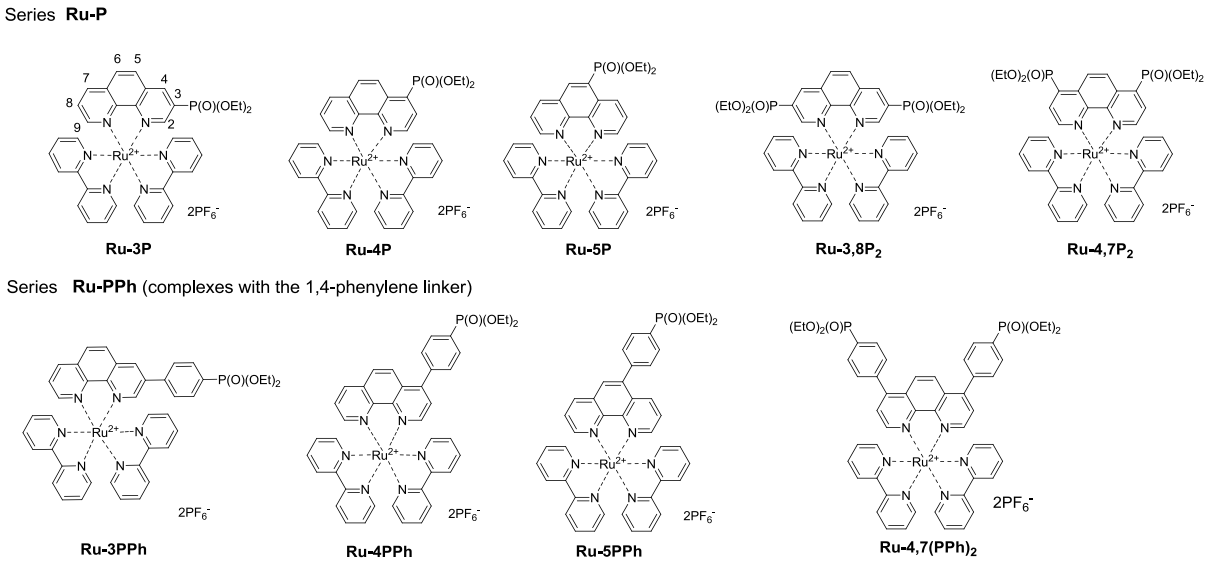

Figure 1. Structures of Ru(II) complexes **Ru-Pcat** investigated in this work.

RESULTS AND DISCUSSION

Synthesis

Phen ligands bearing diethyl phosphonate groups directly attached to the phen core **3P**, **4P**, **5P, 3,8P$_2$** and **4,7P$_2$** were prepared from halogen-substituted 1,10-phenanthrolines using the Hirao reaction as was previously reported by us.[42] Ligands bearing the 1,4-phenylene spacer were obtained as shown in Scheme 1 by using the Suzuki coupling reaction of halogen-substituted 1,10-phenanthrolines and 4-(diethoxyphosphoryl)phenylboronic acid (see Supporting Information).[43] All isomeric mono-substituted derivatives **3PPh**, **4PPh**, **5PPh** and diphosphonate **4,7(PPh)$_2$** were prepared in good yields after optimization of the reaction conditions. The coupling reaction of 4-chloro-1,10-phenanthrolines and 4,7-dichloro-1,10-phenanthrolines smoothly proceeded in the presence of $Pd(OAc)_2/PCy_3$ catalytic system. In contrast, more reactive bromides and $Pd(PPh_3)_4$ catalyst were required for the preparation of 3- and 5-substituted phen ligands. The ^{1}H, ^{13}C and ^{31}P spectra of ligands thus obtained are presented in Figures S36-S47.

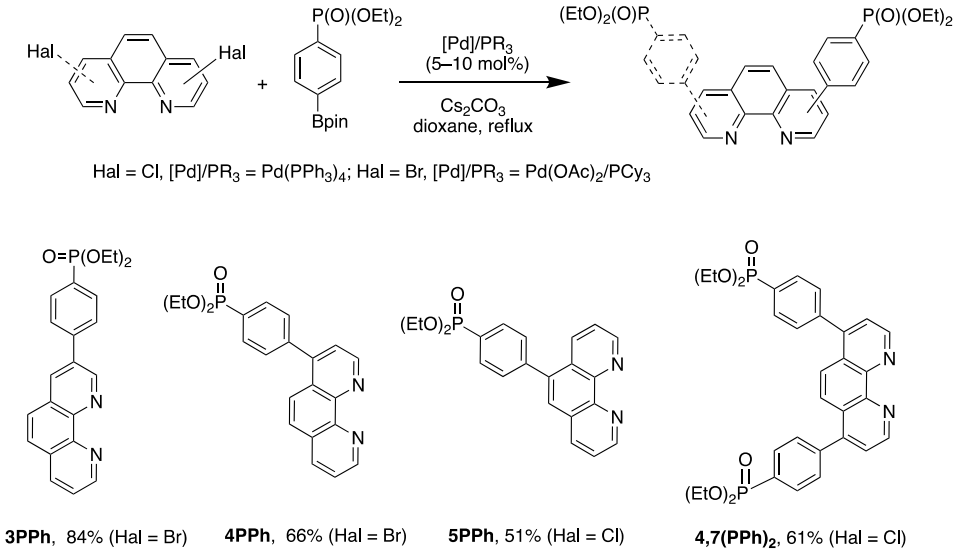

Scheme 1. Synthesis of 4-(diethoxyposphoryl)phenyl-substituted 1,10-phenanthrolines **3PPh**, **4PPh**, **5PPh** and **4,7(PPh)$_2$**.

The synthesis of all Ru(II) complexes described here follows the well-known synthetic approach for preparation of mixed ligand complexes. For each of the ligands, Ru(II) complexes **Ru-Pcat** (Figure 1) were prepared by reacting the ligand and *cis*-$[Ru(bpy)_2Cl_2]\cdot 2H_2O$ in dry ethanol at 100 °C in a MW reactor. All complexes were isolated as hexafluorophosphate salts by the addition of ammonium hexafluorophosphate to partially evaporated reaction mixtures. The complexes were obtained as orange or crimson solids in 50–90% yields, similarly to previously reported for mixed ligand Ru(II) complexes with phen ligands.[16,44]

The purity of **Ru-Pcat** was confirmed during their structural characterization by mass spectrometry and NMR spectroscopy. The successful coordination of phen ligand was confirmed by observation of $[M–PF_6]^+$ ion peak with matching isotopic pattern as the most prominent peak in the high resolution mass spectra.

Complexes **Ru-Pcat** were found to be soluble in polar and protic organic solvents such as chloroform, dichloromethane, THF, ethanol, methanol, acetonitrile, DMF and DMSO.

All compounds **Ru-Pcat** showed high photostability as was proved by irradiating their solutions in acetonitrile or acetonitrile/water (10:1 v/v) solvent mixtures with blue LED for 24 h (Figure S1). Such a high photostability is in agreement with the enhanced photostability of the other reported Ru(II) complexes with electron-withdrawing substituents in bpy ligands.[14] This substituent effect observed in bpy complexes was explained by a decrease in the probability of dd excited states formation, which are prone to the ligand exchange reactions.

Solid-state structures

Additional structural information on the newly synthesized complexes was obtained by single crystal X-ray analysis of representative compounds. Single crystals of **Ru-5P** and **Ru-4,7P$_2$** suitable for X-ray analysis were grown by a slow diffusion of toluene in $CHCl_3$/MeOH solutions of the complexes.

Complexes **Ru-5P** and **Ru-4,7P$_2$** are crystallized in the triclinic space group P-1. A summary of the crystallographic data is given in Table S1 (Supporting Information). The molecular plots of **Ru-5P** and **Ru-4,7P$_2$** are shown in Figure 2 and 3, respectively. Overall, the geometries of these cationic complexes are similar to that of parent **Ru-phen**.[45] The six-coordinated ruthenium center is chelated by nitrogen atoms from two bpy ligands and one phen ligand bearing phosphonate groups and adopts the expected octahedral geometry. Selected bond lengths and angles are reported in the captions of Figures 2 and 3 and in Table S2. All metal nitrogen bond lengths (Ru–N = 2.045–2.067 Å) lay in the usual range[18,44-47] and are almost insensitive to the presence of the phosphonate substituent and its position in the phenanthroline ring. The angles comprising the coordination sphere differ by as much as 11° from the ideal right angles due to the narrow bite angles of these heterocyclic ligands. Dihedral angles between the plane of heteroaromatic ligands and N–Ru–N plane containing nitrogen atoms of this ligand are slightly larger in **Ru-4,7P$_2$** (4.14°, 4.93° and 5.37°) as compared to those observed in **Ru-5P** (1.96°, 2.72° and 5.43°). These deviations were proposed as a criteria of steric hindrance in the coordination environment of Ru center.[44] However, the corresponding parameters of non-substituted complex **Ru-phen** are rather similar to those of **Ru-4,7P$_2$** (Table S2). This led us to conclude that these angles are determined by molecular packing in crystals rather than by the steric hindrance of the metal center.

Thus, the introduction of the $P(O)(OEt)_2$ substituent in 4 and 5 positions of the phen ligand does not significantly change structural parameters of coordination sphere of ruthenium atom.

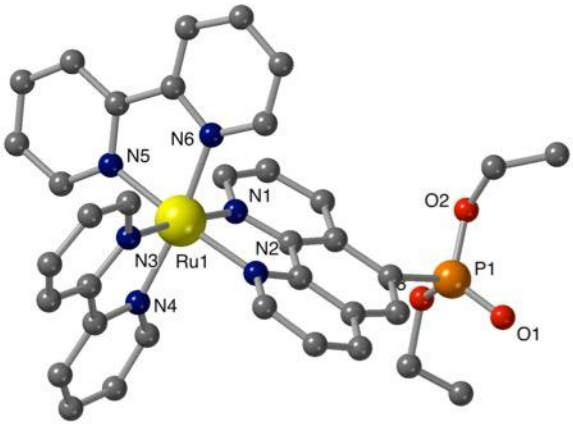

Figure 2. Structure of cationic complex **Ru-5P**. Hexafluorophosphate ions, hydrogen atoms and minor disordered parts are omitted for clarity. Selected bond lengths (Å): Ru–N(1–6) = 2.052(5) – 2.067(5); P=O(1) = 1.451(7); P–O(2,3) = 1.5666(7), 1.5669(6); P–C(7) = 1.799(7).

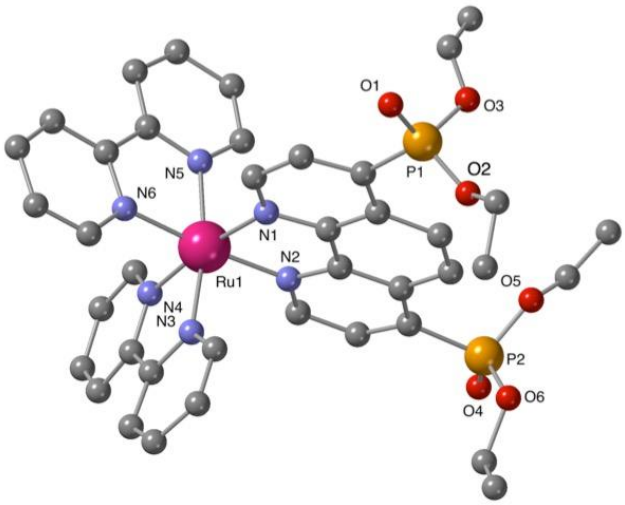

Figure 3. Structure of cationic complex **Ru-4,7P$_2$**. Hexafluorophosphate ions, hydrogen atoms and minor disordered parts are omitted for clarity. Selected bond lengths (Å): Ru–N(1–6) = 2.045(5) – 2.067(5); P=O(1) = 1.489(8); P–O(2,3) = 1.54(1), 1.59(1); P–C(7) = 1.803(6).

Characterization in solution

Kinetic stability and solution structures of studied complexes were confirmed by NMR spectroscopy. Complex **Ru-4P** was chosen as a representative example and investigated in detail in acetonitrile-*d3* solution by NMR spectroscopy. In ^{1}H and ^{13}C{^{1}H} NMR spectra (Figure 4 and S2–S4), characteristic signals of ethoxy groups of P(O)(OEt)$_2$ substituent

display chemical shifts that are similar to those observed in the free ligand **4P**. This is in accordance with crystal structures of **Ru-5P** and **Ru-4,7P$_2$** in which the phosphonate substituent is non-coordinated.

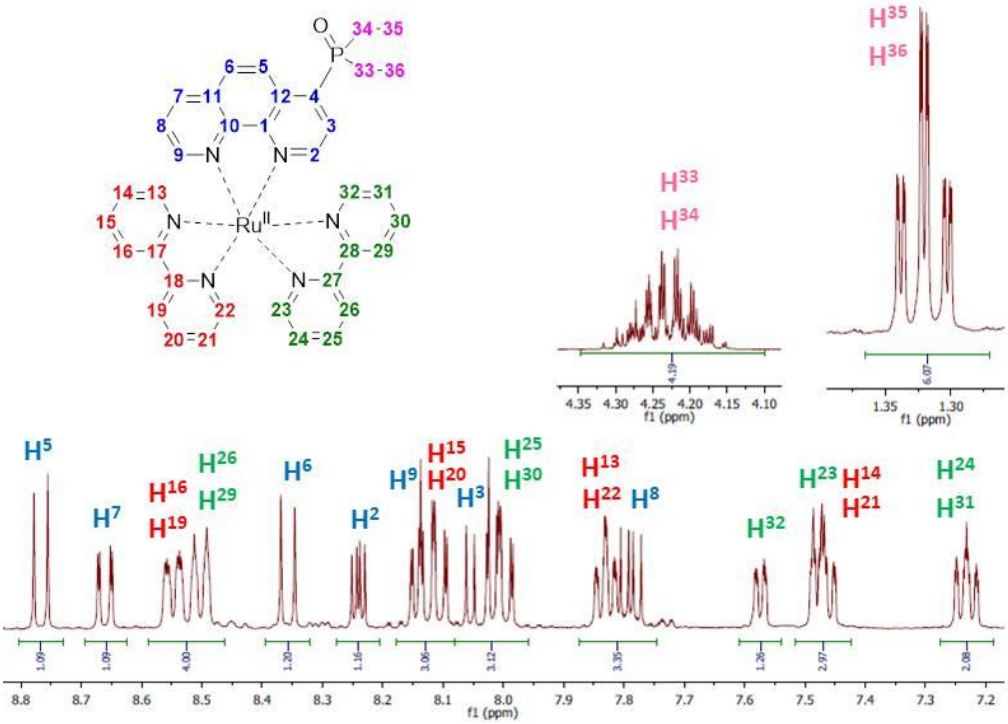

Figure 4. Selected regions of ^{1}H NMR spectrum of **Ru-4P** in acetonitrile-*d3*.

Chemical shifts and coupling constants observed in the ^{1}H NMR spectrum of **Ru-4P** are summarized in Table S3. All proton resonances of the phen ligand were easily attributed using COSY spectrum after the initial assignment of H-3 and H-8 protons (see Figure 4 for proton labels), which appeared as doublets of doublets at δ_H 8.03 and 7.79 ppm with typical coupling constants of $J_{H–H}$ = 5.3 Hz, $^3J_{H–P}$ = 14.7 Hz and $J_{H–H}$ = 5.3 Hz, $J_{H–H}$ = 8.3 Hz, respectively. The remaining 12 signals in aromatic region apparently belong to 16 protons of two bpy ligands. Eight triplets and eight doublets, expected for four pyridine rings, are overlapping but can be distinguished by integration. Four Hα protons of pyridine rings are seen as distinct doublets (δ_H 7.48, 7.57, 7.82 and 7.84 ppm). Three triplets and one doublet have double intensity. The remaining two triplets and two doublets display very similar chemical shifts ($\Delta\delta_H$ < 0.05 in each pair of signals). These paired and strongly overlapped

signals are clearly observed in PSYCHE ^{1}H NMR spectrum (Figure S3b). Using COSY spectrum (Figure S5), four sets of pyridine protons were identified. Their protons H-16, H-19, H-26 and H-29 appeared as two doublets with double intensity and more strongly deshielded in comparison with Hα protons at δ_H 8.50 and 8.54 ppm. The absence of cross peaks through three bands for these protons in gHMBCAD spectrum (Figure S9), enabled their assignment to the protons of two different bpy ligands. This finally allowed for the tentative assignment of two proton sets of bpy ligands.

Surprisingly, all resonances of one bpy molecule are shifted upfield as compared to the corresponding signals of the second bpy ligand. At the same time, the corresponding protons of two pyridine rings in each bpy chelator exhibit identical or very similar chemical shifts and appear as signals with double intensity except those of Hα protons. The only remaining uncertainty at this point is the decision on which of the two bpy ligands is located in *trans* position to the phen ligand.

It is also worth noting that our proton assignment of bpy ligands disagrees with the signals attribution in a series of mixed ligand complexes $[Ru(phen)(bpy)_2]^{2+}$ bearing 5-substituted phenanthrolines, which was reported by Ye et al.[44] and Rau et al.[41] and were based on only COSY measurements and common sense arguments.

All carbon signals observed in ^{13}C NMR spectrum conventionally associated with heterocyclic carbon signals were unambiguously assigned using gHSQCAD (CH carbon atoms) and gHBMCAD (quaternary carbon atoms) spectra (Figures S7–S9). Their chemical shifts and ^{13}C–^{31}P coupling constants are summarized in Table S3. ^{31}P NMR spectrum also proves the non-coordinated character of the phosphonate group.

^{1}H and ^{31}P{^{1}H} NMR spectra of other complexes **Ru-Pcat** are in a good agreement with the proposed structures and are shown in the Supporting Information (Figures S48–S65).

Electrochemistry

Ru-Pcat complexes (Figure 1) were studied by electrochemical methods to assess the effect of substitution pattern on redox potentials and stability of electrogenerated species. The half-wave or peak potential values were obtained from cyclic voltammetry (CV) measurements, which were carried out under N_2 in acetonitrile (MeCN) containing tetra-*n*-butylammonium hexafluorophosphate ($TBAPF_6$, 0.1 M solution) are summarized in Table 1, which also includes the data for reference compounds **Ru-(bpy)$_3$**, **Ru-phen** and **Ru-(phen)$_3$**.

All investigated complexes undergo multiple electron transfers typical for Ru(II) polypyridyl complexes,[48] giving CV curves with up to 6 consecutive ligand–centered reduction and a single oxidation waves observed in the accessible potential window. The CV curves recorded for the **Ru-PPh** series and the reference compound **Ru-phen** are shown in Figure 5.

Table 1. Half-wave and peak potentials (V, *vs* Ag+/Ag) of **Ru-phen, Ru-(phen)$_3$, Ru-(bpy)$_3$** and **Ru-Pcat** complexes in MeCN containing 0.1 M $TBAPF_6$ (vitreous carbon WE ∅ 3mm; 100mV/s).

	Oxidation	Reduction					
	E_{1a}	E_{1c} ($L_1^{0/\bullet-}$)	E_{2c} ($L_2^{0/\bullet-}$)	E_{3c} ($L_3^{0/\bullet-}$)	E_{4c}	E_{5c}	E_{6c}
Ru-phen	0.975 (73)[a]	–1.645 (66)[a]	–1.83 (62)	–2.09 (71)[a]	–2.77[b]	–3.02[b,c]	
Ru-(phen)$_3$	0.975 (71)	–1.68[b]	–1.805[b]				
Ru-(bpy)$_3$	0.97 (75)[a]	–1.64 (62)[a]	–1.83 (57)[a]	–2.075 (61)[a]	–2.76[b]		
Ru-3P	1.03 (80)[a]	–1.45[b]	–1.81 (83)[a]	–2.09 (144)[a]			
Ru-4P	1.025 (73)[a]	–1.415 (63)[a]	–1.78 (63)[a]	–2.01 (61)[a]	–2.40[b]	–2.775[b]	
Ru-5P[c]	1.005 (97)[a]	–1.55[b]	–1.79 (91)[a]	–2.05 (95)[a]	–2.76[b]	–2.89[b]	
Ru-3,8P$_2$	1.08 (94)[a]	-1.23 (73)[a]	–1.71 (77)[a]	–1.92 (68)[a]	–2.2 (75)[a]	–2.83[b]	
Ru-4,7P$_2$	1.08 (99)[a]	–1.335(71)[a]	–1.765 (99)[a]	–1.96 (123)[a]	–2.31[b]	–2.86[b,c]	
Ru-3PPh	0.995 (76)[a]	–1.525 (86)[a]	–1.80 (68)[a]	–2.04 (73)[a]	–2.27 (83)[a]	–2.49 (96)[a]	–2.835[b,d]
Ru-5PPh	0.985 (82)[a]	–1.60 (74)[a]	–1.815 (89)[a]	–2.08 (92)[a]	–2.47[b]	–2.765[b]	
Ru-4,7(PPh)$_2$	0.98 (89)[a]	–1.55 (68)[a]	–1.78 (65)[a]	–2.00 (67)[a]	–2.205 (65)[a]	–2.43 (73)[a]	–2.69 (116)[a]

[a] Half wave potential and [b] peak potential values measured at 0.1 V/s. In our experimental conditions, $E_{1/2}$ [$Fc^{+/}Fc$] = 83 mV. Conversion to SCE-referenced potential values can be obtained by addition of +298mV.[49] [c] Previously reported data for this compound (in DMF, 0.1M Bu_4NBF_4, *vs* $Fc^{+/}Fc$): E_{1a} = 0.75 V, E_{1c} ($L_1^{0/\bullet-}$) = –1.70 V, E_{2c} ($L_2^{0/\bullet-}$) = –2.00 V, E_{3c} ($L_3^{0/\bullet-}$) = –2.20.[41] [d] Broad peak with shoulder.

The effect of the electron-withdrawing $P(O)(OEt)_2$ substituent is first revealed through a shift of the one-electron reversible oxidation wave attributed[50] to the oxidation of the Ru center (Ru^{2+}/Ru^{3+}). As can be seen by comparing the values presented in Table 1, the introduction of $P(O)(OEt)_2$ substituent(s) in one or more of the available positions of the phen core of **Ru-phen** makes the oxidation of corresponding complexes more difficult due to a decrease in the effective charge density at the metal center. The negative inductive effect of $P(O)(OEt)_2$ leads to a 55 and 50 mV shift in $E_{1/2}$ values for **Ru-3P** and **Ru-4P**, respectively, even though in these compounds the substituent remains fairly distant from the metal center (4 and 5 bonds, respectively). Attachment of the second $P(O)(OEt)_2$ group to the opposite pyridine ring (**Ru-3,8P$_2$** and **Ru-4,7P$_2$**) has a similar effect (+50–55 mV per substituent), to

reach an overall positive shift of about +100–105 mV regardless its position. Introduction of the $P(O)(OEt)_2$ in position 5 (complex **Ru-5P**) also influences the oxidation process but leads to a much weaker positive shift in potential (30 mV). Such positive shifts of the first oxidation potentials were already observed in Ru(II) complexes with polypyridyl ligands substituted by electron-acceptors including phosphonate groups.[51] Our results are also in agreement with previous reports demonstrating that there is a strong correlation between $E_{1/2}$ (Ru^{2+}/Ru^{3+}) values and Hammett constants of substituents introduced in position 4 of the pyridine ring.[17]

As expected, the negative inductive effect of $P(O)(OEt)_2$ is significantly lowered when this substituent is separated by a 1,4-phenylene linker in the **Ru-PPh** series. Positive potential shifts of only 10 and 20 mV are observed for **Ru-5PPh** and **Ru-3PPh**. Here again, the amplitude of the shift correlates with the number of bonds introduced between the phosphorous and Ru centers (5 and 4 bonds respectively). Surprisingly, the oxidation potential of the di-substituted complex **Ru-4,7(PPh)$_2$** is found to be shifted by only 5 mV despite the presence of two phosphorous substituents.

As can be seen from Table 1 and Figures 5, S10–S21, numerous reduction waves are observed in the CV curves of the investigated compounds **Ru-P** and **Ru-PPh**, which agrees with the known ability of bpy and phen ligands to undergo two consecutive one-electron reductions in the accessible potential range.[50] We found that the shape and number of these waves depend on the substitution pattern. Six consecutive reversible reduction waves appear well separated in the CV curve of **Ru-3PPh** and **Ru-4,7(PPh)$_2$** while only 5 or 4 waves of different intensities are observed for **Ru-5PPh** and **Ru-Phen**, respectively (Figure 5). Those features are well interpreted as a stepwise reduction of each ligand, with a sequence depending on the relative position of their π* orbitals.[47] The three first waves can be attributed to a stepwise one-electron reduction of the bpy (bpy/bpy$^{\bullet-}$) and phen ligands (phen/phen$^{\bullet-}$). The relative order, and most importantly, the identification the phen-centered reduction among these signals, was determined by comparing the potential values collected with the **Ru-P** series. We found the first reduction wave to be reversible at 100 mV/s for all complexes in this series except for **Ru-3P** and **Ru-5P**, for which partial reversibility could only be observed for scan rates above 2V/s. These two compounds were therefore excluded from the comparison discussed below focusing on the half-wave potential values measured at 100 mV/s for **Ru-4P**, **Ru-3,8P$_2$** and **Ru-4,7P$_2$**. The first three ligand-based reductions noted E_{1c} ($L_1^{0/\bullet-}$), E_{2c} ($L_2^{0/\bullet-}$) and E_{3c} ($L_3^{0/\bullet-}$) are observed in the range of –1.23 to –1.415 V (ΔE = 185 mV), –1.71 to –1.81 (ΔE = 100 mV), and –1.92 to –2.01 (ΔE = 90 mV), respectively. A

rapid overview of those data reveals that the introduction of one or two EWGs on the phen ligand is mainly reflected in the shifts of the first reduction wave, with a maximum value of about 185 mV observed between **Ru-4P** and **Ru-3,8P$_2$**. It should also be noted that there is a rather large shift of about 100 mV between the E_{1c} values calculated for the isomeric complexes **Ru-4,7P$_2$** and **Ru-3,8P$_2$**, which is consistent with the above conclusion that the inductive effect is stronger when the substituent is introduced in position 3. We also found that the first reduction waves systematically appear at significantly lower potentials than those of the reference complexes **Ru-(bpy)$_3$** and **Ru-phen** reduction. All these data led us to attribute the first wave observed at E_{1c} ($L_1^{0/\bullet-}$) to the one-electron reduction of the phen ligand and the two following ones E_{2c} ($L_2^{0/\bullet-}$) and E_{3c} ($L_3^{0/\bullet-}$) to the reduction of the bipyridines.

This hypothesis is indirectly supported by the irreversible character of the first reduction waves in the CV curves of **Ru-3P** and **Ru-5P** complexes which is attributed to the existence of a chemical step coupled to formation of phen$^{\bullet-}$ species. This instability resulting from the presence of a single EWG at positions 3 or 5 is currently not understood and all the more surprising since it is not observed for **Ru-4P** and the disubstituted derivatives under the same conditions.

It should be noted that the proposed attribution strongly differs from the experimental data for **Ru-phen** and theoretical studies so far reported for mixed Ru(II) complexes, containing bpy and phen ligands, suggesting that the bpy ligand is easier to reduce than the phen.[52,53] These reported observations are consistent with our experimental data collected with the reference **Ru-(bpy)$_3$**, **Ru-(phen)$_3$** and **Ru-phen** complexes (Table 1) showing that the reduction of the phen ligand is only slightly negatively shifted (by about −40 mV) compared to that of bpy and that the largest difference between the **Ru-(bpy)$_3$** and **Ru-phen** complexes is observed in the third reduction process E_{3c} ($L_3^{0/\bullet-}$). Our attribution of the first wave in **Ru-P** to the phen-centered reduction is easily understood taking into account the strong EW character of P(O)(OEt)$_2$ group which makes the reduction of the phen ligand much easier than that of the unsubstituted bipyridines.

In the **Ru-PPh** series, the first reduction potentials E_{1c} ($L_1^{0/\bullet-}$) are also positively shifted and more sensitive to substitution than E_{3c} ($L_3^{0/\bullet-}$) with the exception of **Ru-4,7(PPh)$_2$**. Thus, the attribution of the reduction peaks in this series using this criterion is ambiguous. Comparison of potential values obtained for **Ru-3PPh**, **Ru-5PPh** and **Ru-phen** provides however strong support of our hypothesis that the electron is also localized on the phen ligand for these reduced complexes.

Spectroelectrochemistry (SEC) measurements can provide useful information for deciphering reduction mechanisms involved in ruthenium(II) mixed-ligand complexes.[52] Attribution of the first reduction wave to the reduction of the phen ligands in the **Ru-P** series was thus further supported by SEC. These measurements were carried out in thin-layer cells upon collecting time-resolved UV–vis spectra during the first reduction of selected compounds. The curves obtained for **Ru-4P**, **Ru-4,7P$_2$**, **Ru-(bpy)$_3$** and **Ru-(phen)$_3$** are shown in Figure 6. The one-electron reduction of **Ru-4P** and **Ru-4,7P$_2$** leads to similar changes including the development of a broad and intense band in the range 460–480 nm range with a shoulder at about 600 nm. These features contradict with those collected under the same conditions for the reference compound **Ru-(bpy)$_3$**, where the first reduction of the bpy ligand leads to the appearance of more red shifted signals above 500 nm along with additional weak signals at about 784 and 867 nm. Appearance of the broad absorption band at shorter wavelength (600–650 nm) is a characteristic signature of phen$^{\bullet-}$ radical anion as reported previously[52] and confirmed by us for **Ru-(phen)$_3$**.

Altogether, the electrochemical and spectroelectrochemical data discussed above reveal that the addition of P(O)(OEt)$_2$ group to **Ru-phen** leads to a large positive shift of the first reduction wave whose magnitude depends on the substitution pattern. The two following bpy-centered reduction waves as well as the Ru-centered oxidation wave are also affected but to a much lesser extent in most of the complexes. Greater sensitivity of the ligand-based reductions as compared to the metal-based oxidation can be explained by the localization of the P(O)(OEt)$_2$ substituents in the ligand. We also found that the addition of a phenylene linker between the phen core and the P(O)(OEt)$_2$ group lowers the substituent effect on the reduction potentials and can be used for fine tuning of redox potentials. Most importantly all collected data demonstrate that the first electron transfer is centered on the phen ligand in **Ru-P** and most probably in **Ru-PPh** series in contrast to the parent complex **Ru-phen**. We can expect that the localization of the first electron transfer on the phen ligand in **Ru-Pcat** could have a great influence on both photophysical and photocatalytic properties of these complexes.

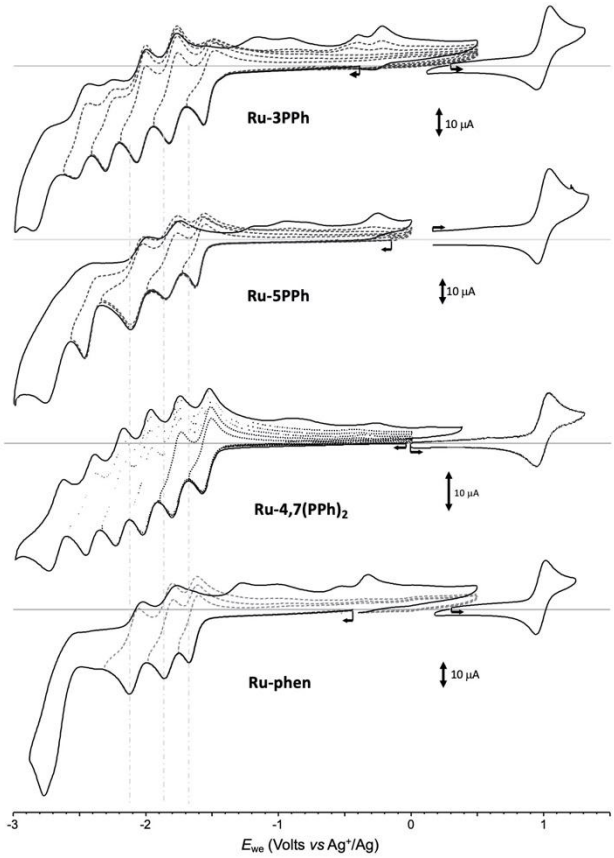

Figure 5. Voltamperometric curves of MeCN solutions of **Ru-3PPh**, **Ru-5PPh**, **Ru-4,7(PPh)$_2$** and **Ru-Phen** (1x10^{-3} M + 0.1M in TBAPF$_6$) recorded at a vitreous carbon working electrode (Ø = 3 mm, 0.1 V s^{-1}).

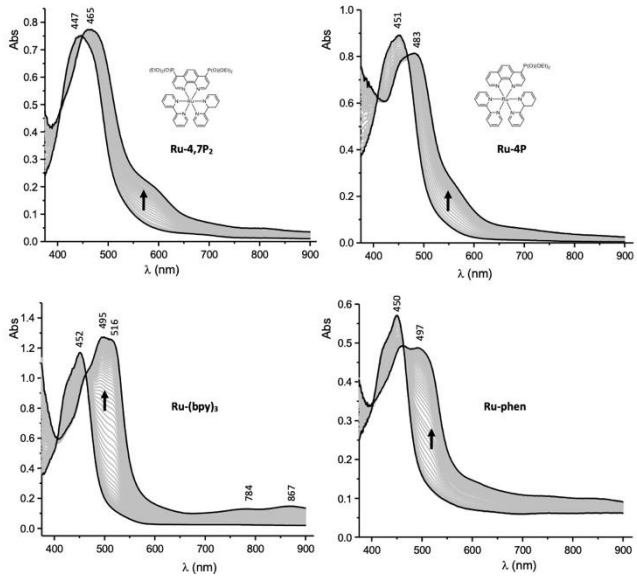

Figure 6. UV–vis spectra recorded during the first one-electron reduction of **Ru-4,7P$_2$**, **Ru-4P**, **Ru-(bpy)$_3$** and **Ru-phen** in MeCN containing 0.1M TBAPF$_6$ (working electrode: Pt, *l* = 0.5 mm).

Photophysical properties

The electronic absorption and emission spectra of newly synthesized **Ru-Pcat** complexes and reference compounds in MeCN are presented in Figure S22 and summarized in Table 2. All complexes exhibit intense absorption bands in the 250–350 nm region, which can be assigned to the ligand-centered π–π* electronic transitions.[54,55] The spectra also show characteristic broad absorption bands in the longer wavelength region (400–500 nm) due to overlapping spin-allowed metal–to–ligand charge transfer (MLCT) and interligand bpy/phen-based charge transfer (LLCT) transitions. The observed absorption bands are broader compared to those of the reference **Ru-phen** complex (Figure 7) probably due to an increased number of MLCT and LLCT transitions between bpy and phosphorylated phen ligands.[15,56] Positions of the absorption maxima for **Ru-Pcat** are relatively insensitive to the substitution pattern in phen ligand, except for (3-phosphonate)-substituted derivatives. For complexes **Ru-3P** and **Ru-3,8P$_2$**, the lower energy transition is shifted to shorter wavelengths (443 and 435 nm, respectively) compared to **Ru-phen** (450 nm). Additional low intensity shoulder at 481 nm was observed for **Ru-3,8P$_2$** in line with previous reports on Ru(II) complexes with phen ligands.[57-60]

All studied complexes exhibit rather intense luminescence emission at room temperature which is strongly quenched in the presence of oxygen (Figure S22). A broad structureless emission band with maximum at 605 nm was observed for 5-substituted compounds **Ru-5P** and **Ru-5PPh** similarly to **Ru-phen**. Introduction of a single phosphonate group in positions 3 and 4 resulted in a strong red shift (256410–285714 cm^{-1} (35–39 nm)) of the emission maxima. Such red shift of the emission is commonly observed for Ru(II) complexes with ligands bearing electron-withdrawing substituents.[14] Surprisingly, the second phosphonate substituent strongly further redshifts the emission band (285714 cm^{-1} (53 nm)) only if this substituent is introduced in position 8. The luminescence band of **Ru-4,7P$_2$** (651 nm) is red-shifted by only 1000000 cm^{-1} (10 nm) relative to that of **Ru-4P** complex. Emission quantum yield values (Φ_{em}) of all complexes bearing the phosphonate group in phen ring (Series **Ru-P**, Figure 1) are comparable with those of **Ru-bpy** (0.095) and **Ru-phen** (0.096), except for **Ru-3,8P$_2$** (0.021).

For complexes with a phenylene linker (**Ru-PPh** series, Figure 1), the observed red shifts are substantially smaller compared to correspondingly substituted complexes in **Ru-P** series. At the same time, the emission quantum yields fall in the range of 0.121 to 0.253 reaching the maximum for **Ru-4,7(PPh)$_2$** that is about 2.5-fold higher than Φ_{em} of **Ru-phen**.

Such high quantum yields values were previously reported for di-aryl-substituted phen complexes represented here by **Ru-4,7Ph$_2$** (Table 3).[59] Notably, introduction of the phosphonate substituent in the phenyl ring allowed for a significant increase (from 0.155 to 0.253) of the luminescence quantum yield and hydrophilicity of complex **Ru-4,7Ph$_2$**, which was actively investigated as a valuable DNA marker.[61,62]

The apparent Stokes shifts for the complexes of both series are comparable to that of the parent **Ru-phen** (64516 cm^{-1}), except for compounds bearing phosphonate group in position 4 and **Ru-3,8P$_2$**, for which they are increased in the following order: **Ru-4,7(PPh)$_2$** (59172 cm^{-1}) < **Ru-4P** (51546 cm^{-1}) < **Ru-4,7P$_2$** (47847 cm^{-1}) < **Ru-3,8P$_2$** (46296 cm^{-1}).

Thus, absorption and particularly emission of [Ru(phen)(bpy)$_2$]$^{2+}$-type complexes can be fine-tuned by varying the number and position of P(O)(OEt)$_2$ groups in the phen ring. Complex **Ru-3,8P$_2$** is interesting as it is the only example in **Ru-Pcat** series that exhibits an emission band in the first near IR region. In contrast to previously reported[29,34] complexes bearing the phosphonate group in the bpy ring, the introduction of this substituent in the phen core decreases the emissivity of the resulting Ru(II) complexes only in the case of **Ru-3,8P$_2$**. Emissive properties are generally related to the efficiency of photooxidation reactions mediated by molecular oxygen.[63] Thus, **Ru-3,8P$_2$** seems to be a less promising candidate for photocatalytic oxidation reactions studied in this work.

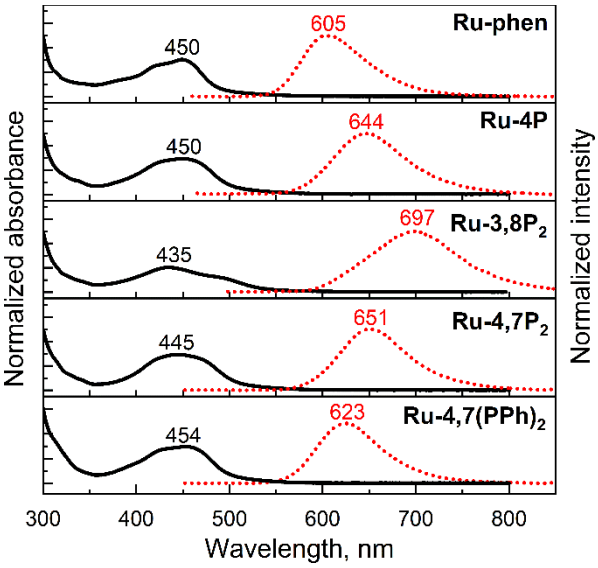

Figure 7. Absorption (black solid line) and emission (red dotted line) spectra of representative **Ru-Pcat** complexes and reference compound **Ru-phen** in deaerated MeCN. Emission was excited at 450 nm.

Table 2. Selected photophysical parameters and quantum yield of singlet oxygen generation (Φ_Δ) for **Ru-(bpy)$_3$**, **Ru-phen** and **Ru-Pcat** complexes.

Compound	λ_{abs} (nm) ($\varepsilon \cdot 10^{-3}$ (M^{-1} cm^{-1}))	λ_{em} (nm) [a]	Φ_{em} [b]	Φ_Δ [c]
Ru-(bpy)$_3$	451 (14.0), 286 (85.0)	609	0.095	0.57
Ru-phen	450 (12.1), 283(49), 272 (42)	605	0.096	0.54
Ru-3P	443 (13.5), 285 (63.9), 268 (65.4)	641	0.078	0.65
Ru-4P	450 (14.1), 283 (58.0), 272 (59.0)	644	0.085	0.53
Ru-5P[d]	449 (16.2), 285 (62.2), 265 (58.0)	603	0.126	0.55
Ru-3,8P$_2$	481 (6.8), 435 (10.2), 284 (52.0), 272 (62.0)	697	0.021	0.28
Ru-4,7P$_2$	445 (17.4), 261(85.0)	651	0.101	0.74
Ru-3PPh	453 (13.0), 283 (80.0)	614	0.121	0.68
Ru-4PPh	453 (17.5)	613	0.181	0.75
Ru-5PPh	450 (14.6), 285 (59.0)	606	0.121	0.61
Ru-4,7Ph$_2$[e]	454(19.9), 284 (90.7)	614	0.155	-
Ru-4,7(PPh)$_2$	454 (18.0), 278 (90.0)	623	0.253	0.73

[a] Emission was excited at 450 nm. [b] Measured in deaerated acetonitrile at ambient temperatures relative to a solution of **Ru-(bpy)$_3$** as a standard.[64] [c] Measured in air-saturated acetonitrile using **Ru-(bpy)$_3$** as a reference photosensitizer.[65] [d] Previously reported data for this compound : λ_{abs} ($\varepsilon \cdot 10^{-3}$) 450 (15.08), 287 (56), 265 (51) nm (M^{-1} cm^{-1}); λ_{em} = 601 nm.[41] [e] **Ru-4,7Ph$_2$** = bis(2,2′-bipyridine)(4,7-diphenyl-1,10-phenanthroline)ruthenium(II) hexafluorophosphate. Taken from ref. [53].

This conclusion was proved by measuring of singlet oxygen quantum yields (Φ_Δ) for complexes **Ru-Pcat** using chemical trapping method with 1,9-dimethylanthracene (DMA) in acetonitrile. Upon irradiation of air-saturated solutions containing each complex at 488 nm, DMA selectively reacts with singlet oxygen forming corresponding endoperoxide. **Ru-Pcat** complexes showed no absorption change in the course of irradiation (Figure S23). The change of DMA absorbance with time is linear (Figure 8, inset), allowing to obtain Φ_Δ value from comparison with the reference **Ru-(bpy)$_3$**. All complexes displayed excellent ability to generate singlet oxygen with Φ_Δ value comparable or higher than those of referenced photosensitizers **Ru-phen** and **Ru-(bpy)$_3$** (0.54 and 0.57, respectively). For 4 and 7-substituted complexes, Φ_Δ values reach up to 0.75 with the exception for **Ru-4P**. It is worth to note that these values are comparable with those of conventional organic photosensitizers such as Methylene Blue (0.5) and Rose Bengal (0.8).[66] Thus, **Ru-Pcat** complexes are promising photocatalysts for oxidation of organic compounds by molecular oxygen.

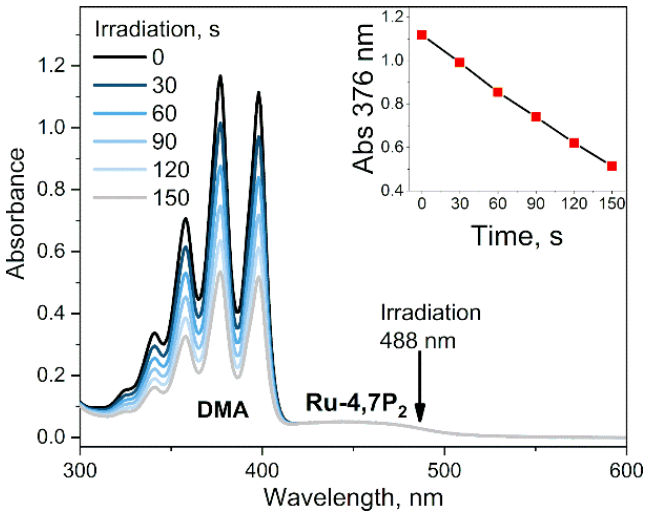

Figure 8. Example of photosensitized oxidation of 1,9-dimethylanthracene in the presence of **Ru-4,7P$_2$** in air saturated acetonitrile solution irradiated with 488 nm laser (10 mW cm^{-2}). Inset: change of absorbance at 376 nm with time.

DFT studies

To get insight into electronic structure of complexes **Ru-Pcat**, DFT calculations were carried out on all complexes with the Firefly quantum chemistry package,[67] which is partially based on the GAMESS (US)[68] source code. The calculations were performed using B3LYP functional with STO 6-31G(d,p) basis set for all elements except Ru, for which we used the Stuttgart valence basis set and pseudopotential.[69] The optimized geometries of complexes **Ru-Pcat** are depicted in Figures S24–S33 and calculated structural parameters are summarized in Table S4 (see the Supporting Information). A satisfactory agreement of calculated and experimental data was observed for complexes **Ru-5P** and **Ru-4,7P$_2$** (Table S4).

Isodensity plots of HOMO and LUMO orbitals of representative complexes **Ru-P** and **Ru-PPh** along with a diagram showing HOMO and LUMO energy levels are presented in Figure 9. A set of π* orbitals associated with phen and bpy ligands are close in energy and the highest-energy occupied orbitals also give a set with very similar energies due to small contributions of ligands in these orbitals wherein the electron density is found primarily on the metal center. This is consistent with broad light absorption manifold observed in the experimental spectra.

There is no orbital mixing for the phenanthroline scaffold and P(O)(OEt)$_2$ substituent in boundary orbitals for complexes of **Ru-P** series, and the energies of HOMO and LUMO orbitals are varying in only a slight extent depending on the substitution pattern (Tables S5–

S10). By comparing boundary orbitals of phosphonate-substituted complexes to those of the parent **Ru-phen** complex a close similarity can be noticed when one or two phosphonate substituents are attached to position 4 and 5 of the phen ring (**Ru-5P**, **Ru-4P** and **Ru-4,7P$_2$**) (Figure 9 and Tables S5–S8). As shown in Figure 9 for complex **Ru-4P**, the main contribution to HOMO, HOMO–1 and HOMO–2 comes from d orbitals but there is also a partial ligand character in particular for HOMO–1 (phen ligand) and HOMO–2 (bpy ligand). The LUMO and LUMO+1 levels are situated on both bpy ligands, while the π* orbitals of the phen ligand give the main contribution to LUMO+2 and LUMO+3.

The HOMOs of **Ru-3P** and **Ru-3,8P$_2$** are very similar to those of other **Ru-P** complexes that is expected because the substituent is still quite distant from the metal d orbitals which are the main contributors to HOMOs (Tables S8 and S10). In contrast, the electron density of LUMO of **Ru-3P** is found on π* orbitals of all three heteroaromatic ligands. Significant phen and bpy character is also observed in LUMO+1 and LUMO+2 despite the electron density is delocalized on only two ligands in both orbitals. The electron density distribution in LUMOs of **Ru-3,8P$_2$** resembles to that of **Ru-phen** with only one exception that the order of LUMOs situated on π* orbitals of bpy and phen ligands is changed. In **Ru-3,8P$_2$**, LUMO and LUMO+3 are localized mainly on the π* orbitals of the phen ligand while the electron density of other two unoccupied boundary orbitals is found on bpy ligands. Accordingly, the energies of MLCT and LLCT transitions in 3-substituted derivatives can be significantly different from those observed in other **Ru-P** complexes as it is experimentally observed in electronic absorption and luminescence spectra.

Ru(II) complexes with the phenylene linker (**Ru-PPh**) differ from the parent complex **Ru-phen** in the character of HOMOs orbitals. The main contribution to the HOMOs comes from π orbitals of the phenylene linker and the phosphonate substituent. The electron density is found mainly on d orbitals only at HOMO–3 level for **Ru-5PPh** and HOMO–2 and HOMO–3 for **Ru-3PPh** and **Ru-4PPh** (Table S11–S13). In complex, **Ru-4,7(PPh)$_2$**, all HOMOs are constructed from d orbitals and π orbitals of the phenylene linker and the phosphonate substituent with small amount of electron density observed on d orbitals (Table S14). In contrast, their LUMOs are rather similar to those of **Ru-phen**.

It is known that the presence of low-lying dd states can strongly decrease excited-state lifetimes and photostability of Ru(II) complexes.[14] The absence of such states in all studied complexes is likely to account for their high photostability. In contrast, our attempt to use the calculated MO energies for deeper understanding the oxidation and reduction potentials

showed a limited value of such simple DFT calculations. Complex **Ru-3,8P$_2$** was the only compound, for which DFT calculations agree with the assignment of the first reduction potentials discussed above. We tried to overcome the inconsistence of experimental and theoretical data by changing STO 6-31G(d,p) basis to CRENBL, LANL2DZ or Stuttgart 1997 RSC ECP for ruthenium atom and to Jorge-TZP for other atoms and also compared our results with data reported by other groups.[23, 32, 53, 70] All our calculations gave similar electron density distributions in boundary orbitals for **Ru-phen** and were comparable to the previously reported data. Similar inconsistences of experimental and calculated data were already discussed by others.[70] Also we have not attempted to perform computations of excited states by TD-DFT method. Our previous experience as well as common knowledge say that this method, though quite reasonable in the computations of organic chromophores and coordination compounds involving the transitions of purely ligand-to-ligand nature, tends to give inconsistent if not merely ridiculous predictions when it comes to states including heavy transition metals of 2-nd and 3rd rows. At the same time going beyond TD-DFT to more sophisticated levels of theory is far beyond our current computational facilities.[71-74]

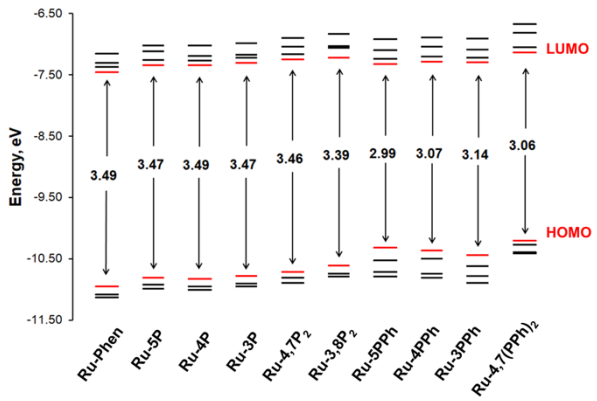

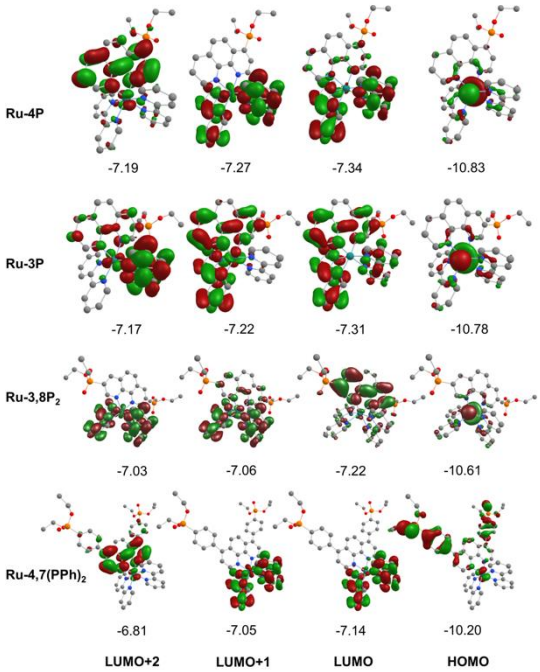

Figure 9. (Top). Frontier orbital energies obtained from DFT calculations for **Ru-cat**. (Bottom) The isodensity plot of HOMO and LUMO orbitals for the representative set of chromophores **Ru-cat** obtained from DFT calculations illustrating effects of ligand substituents.

Photocatalytic properties

Visible light-promoted reactions are started with absorption of a photon by a photocatalyst PC), leading to generation of an excited state *PC. Thus formed, the high energy species *PC can take part in chemical transformations, which happens due to either energy transfer (the EnT photocatalysis) or electron transfer (the redox photocatalysis or photoredox catalysis) to substrates or oxidative or reductive quenchers. Rapid insight into efficiency of a photocatalyst in both types of processes is possible by using specific experimental and calculated parameters.

The EnT photocatalytic reactions are less common and most of them involve oxidation reactions by molecular oxygen.[7,75] Energy transfer from an excited ruthenium(II) complex to oxygen molecule can generate singlet oxygen (Scheme 2, pathway A, eq. 2) and this step is usually the rate-limiting in oxygenation reaction. Thus, singlet oxygen quantum yield (Φ_Δ) (Table 2) is prerequisite for preliminary evaluation of photocatalyst's efficiency in oxidation reactions.

The ability of Ru(II) complexes to initiate electron transfer after absorption of a photon depends on redox potentials of excited species, while further evolution of catalytic

cycle may involved redox-reactions of the ground states.[10,76] Since excited Ru(II) complexes can be involved in both reductive and oxidative quenching photocatalytic cycles, both first oxidation and reduction potentials of the excited and ground states influence the performance in photoredox catalysis. The redox potentials of the ground state are available from electrochemical studies. Formal redox potentials of the excited state can be estimated by different methods[70,77] and simplified calculations[76,77] based on CV and spectroscopic data are commonly used in organic photocatalysis. The data obtained for the **Ru-Pcat** complexes are summarized in Table S15. On comparing the redox potentials of phosphorous-substituted complexes **Ru-P**, it can be concluded that the substitution pattern does influence all redox potentials and that the introduction of EWG can be expected to favor the reductive quenching photocatalytic cycle.

It is also worth mentioning that most phosphonate-substituted complexes **Ru-Pcat** exhibit similar absorption manifolds in the region covered by blue LED, allowing to safely ignore probable effects of the difference in absorptivity on their photocatalytic activity thus simplifying their comparison in photocatalytic reactions.

To investigate the catalytic properties of **Ru-Pcat**, the oxidation of sulfides into sulfoxides by molecular oxygen was chosen as a model reaction. This reaction attracts considerable interest due to its relevance to biochemistry, warfare agents disposal, environmental consequences of fuel desulfurization and in organic synthesis.[78-84] The overoxidation of sulfides to sulfones and the cleavage of S–C and (S)C–H bonds are commonly observed as side reactions[85-87] and thus selective methods for transformation of different sulfides are in high demand in particular in asymmetric synthesis and in the development of pharmaceuticals involving selective late-stage oxygenation.[83,88] Explosive peracids and peroxides are commonly used in industry to prepare sulfoxides and sulfones on large scale.[89] Their replacement by less dangerous reagents in the production of fine chemicals is highly desirable. Photocatalysis allows to perform these oxidation reactions using molecular oxygen as a terminal oxidant. We have chosen this reaction as a model reaction to study photocatalytic properties of **Ru-Pcat** not only due to its practical importance but also because the reaction mechanism was thoroughly investigated at least in the case of organic photocatalysts[75,90-92] that simplifies understanding of substituent effects on the reaction course.

It was shown that the photooxidation of sulfides by oxygen proceeds through either of two mechanisms.[75,90-92] The reaction can be initiated by energy transfer from the excited-state photocatalyst (*PC) to oxygen molecule (Scheme 2, pathway A) or by electron transfer from

sulfide molecule to the excited-state PC (Scheme 2, pathway B). Alkyl sulfides are commonly oxidized by the generated singlet oxygen ($^1O_2$), while aryl sulfides tend to react through both mechanisms with most of organic photocatalysts.[91,93-95] We decided to evaluate the performance of our complexes in redox and EnT photocatalytic reactions by studying sulfoxidation of aryl sulfides and alkyl sulfides, respectively.

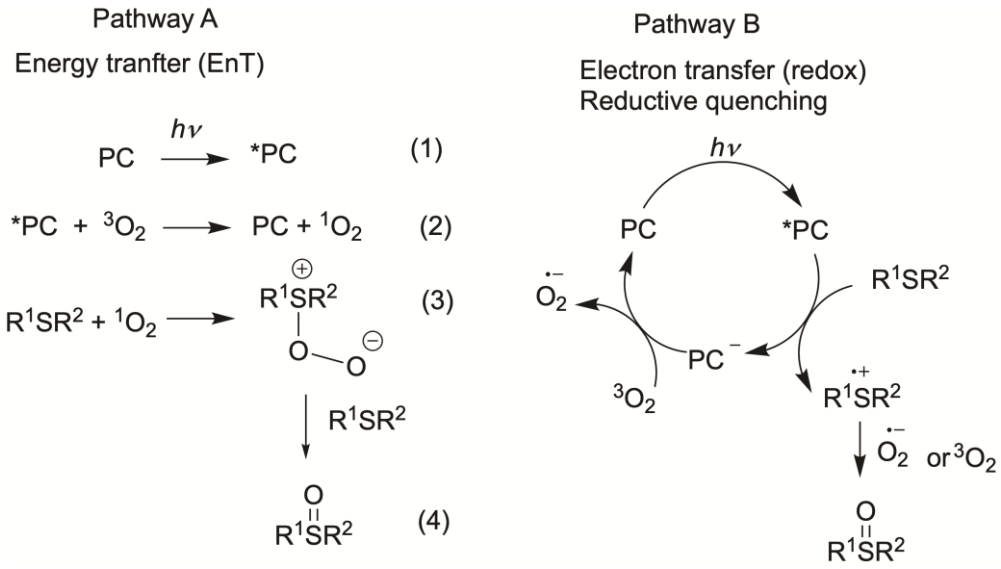

Scheme 2. Two possible pathways for of the photooxidation of sulfides by molecular oxygen.

First, photocatalytic efficiency of Ru(II) complexes in this reaction was investigated (Scheme 3). Dialkyl sulfides and methyl aryl sulfides can be quantitively oxidized by slowly bubbling molecular oxygen through their solution in MeCN/H_2O (10:1 v/v) mixture containing **Ru-phen** or **Ru-(bpy)$_3$**. In contrast to the previously reported oxidation in chloroform saturated by water,[96] under these conditions the reaction proceeded selectively even for the most problematic methyl benzyl sulfide,[86,97,98] for which the side reactions of C–S and (S)C–H cleavage are commonly observed.[86,97,98] The oxidation was not observed in the absence of water and without irradiation of the reaction mixtures. Dialkyl sulfides were found to be more reactive than aryl sulfides and gave the products quantitively in less than 4 h with the amount of catalyst as low as 0.005 mol%. As in the case of organic photocatalysts, the rate of oxidation of aryl methyl sulfides depended on the substitution in the aromatic ring, and electron acceptor groups at phenyl ring decreased the reaction rate. Nevertheless, increasing the amount of photocatalyst up to 0.05 mol% allowed for oxidation of aryl methyl sulfides to

obtain target sulfoxides in quantitative yield within 6 h of irradiation. However, diphenyl sulfide didn't react under these conditions even after increasing the loading **Ru-phen** and **Ru-(bpy)$_3$** up to 2 mol%. Sulfoxides thus obtained can be easily isolated in pure form (> 98%) without additional purification by column chromatography. All complexes **Ru-Pcat** were found to be efficient in these reactions and gave the target sulfoxides in quantitative yields.

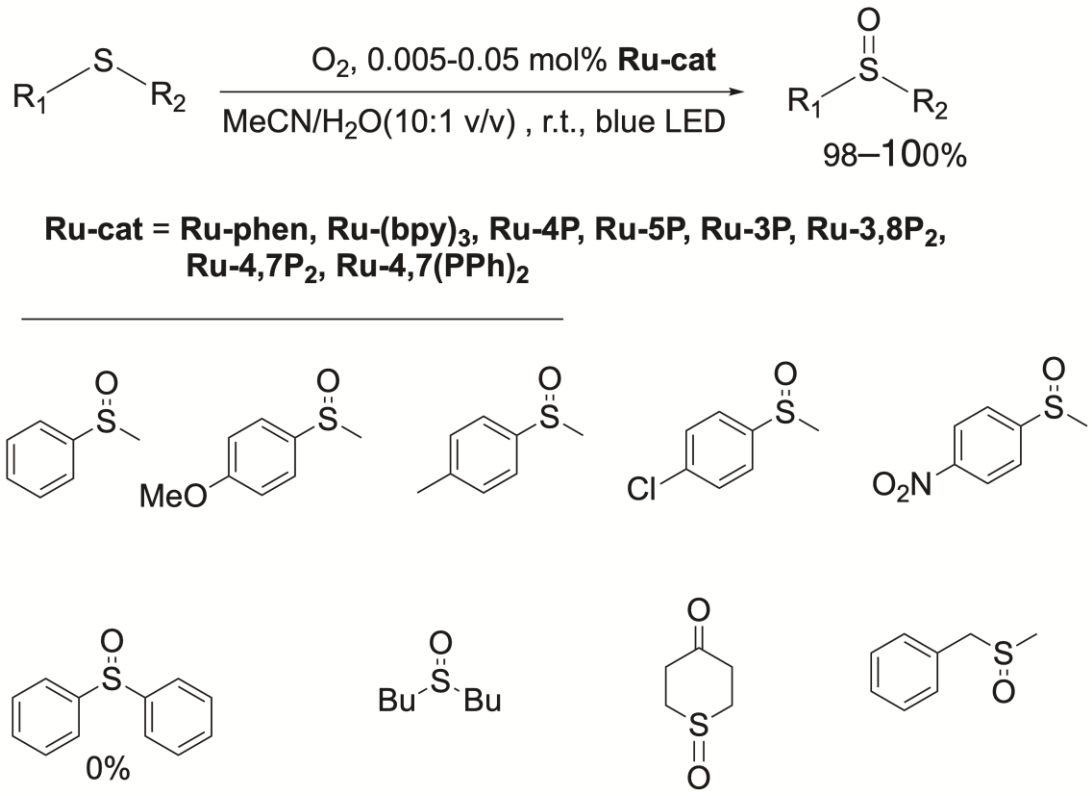

Scheme 3. Photocatalytic synthesis of sulfoxides using molecular oxygen as an oxidant.

Encouraged by these results, we undertook kinetic studies to understand the substituent effects on the efficiency of **Ru-Pcat** complexes. All starting sulfides, complexes and the reaction products were soluble in MeCN/H_2O (10:1 v/v) solvent mixture that allowed for measuring the reaction rates by NMR spectroscopy after withdrawing aliquot samples. The change of conversion over time for the oxidation 4-nitrothioanisole in the presence of 0.05 mol% **Ru-Pcat** is shown in Figure 10. The substitution pattern does influence the reaction rate. In the series of isomeric mono-substituted derivatives **Ru-P**, acceleration of the oxidation was observed in the following range: **Ru-5P** ≤ **Ru-phen** < **Ru-3P** < **Ru-4P** and the most efficient **Ru-4P** complex provided the complete conversion by about 2.5-fold more rapidly than **Ru-phen** and commonly used **Ru-(bpy)$_3$**. The positive effect of the second

phosphonate substituent was less pronounced but still observable when the **Ru-4P** photocatalyst was replaced by **Ru-4,7P$_2$**. In contrast, **Ru-3,8P$_2$** was less efficient than **Ru-3P**. The introduction of phenylene linker between the aromatic ring and the P(O)(OEt)$_2$ group had a detrimental effect on the reaction rate as was evident from comparing **Ru-4,7P$_2$** and **Ru-4,7(PPh)$_2$** photocatalysts.

The high efficiency of **Ru-4P** and **Ru-4,7P$_2$** derivatives as compared to **Ru-(bpy)$_3$** and **Ru-phen** complexes in this oxidation reaction (which predominantly proceeds through the reductive quenching catalytic cycle (pathway B, Scheme 2)) can be explained by higher values of their $E_{1/2}$(*PC/PC$^-$) potentials. However, correlation between the oxidation rate and this parameter is not as clear for mono-substituted derivatives **Ru-3P** and **Ru-4P**, exhibiting the markedly different photocatalytic efficiency while rather similar $E_{1/2}$ (*PC/PC$^-$) values. This is also understandable because the reduction potential of the excited complex represents an approximative criterion for evaluation of reaction thermodynamics while kinetics often determines the processes involving short-lived intermediates. On the other hand, we cannot exclude that non-linearity between the reaction rate and redox potentials observed for the **Ru-P** photocatalysts results from small but noticeable contribution of singlet oxygen in the reaction outcome (Pathway A, Scheme 2).

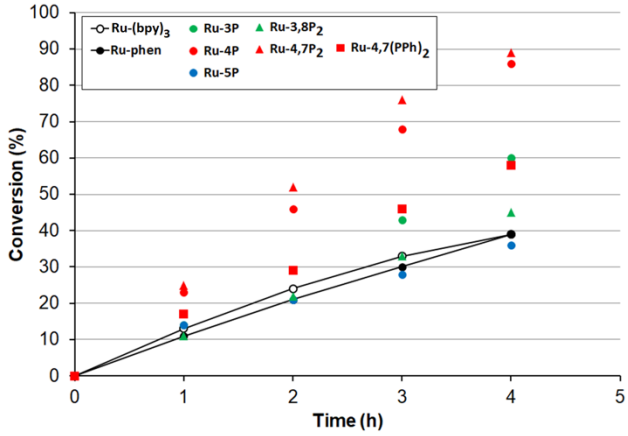

Figure 10. Photooxidation of 4-nitrothioanisol by molecular oxygen in the presence of 0.05 mol% **Ru-Pcat** and referenced photocatalysts **Ru-(bpy)$_3$** and **Ru-phen** in MeCN/H$_2$O (10:1 v/v) under irradiation of blue LED.

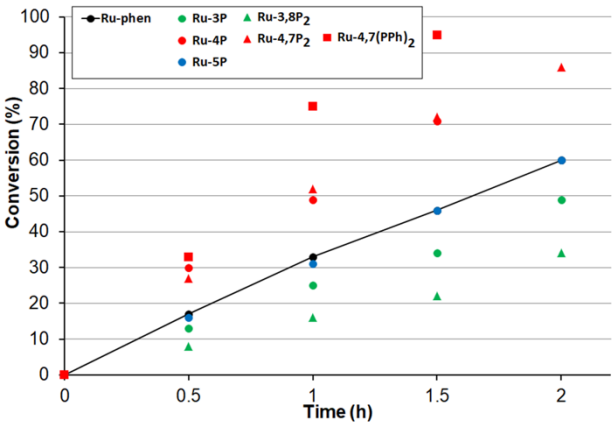

Figure 11. Photooxidation of dibutyl sulfide by molecular oxygen in the presence of 0.005 mol% **Ru-Pcat** and referenced photocatalysts **Ru-(bpy)$_3$** and **Ru-phen** in MeCN/H_2O (10:1 v/v) under irradiation of blue LED.

Next, the oxidation of dibutyl sulfide was investigated because the singlet oxygen mechanism is considered to be operative for this substrate. This sulfide was more reactive than 4-nitroanizole, and the photocatalyst loading was decreased by a factor of 10 to obtain comparable oxidation rates for both sulfides. This indicates that singlet oxygen is an oxidant in this reaction because bimolecular quenching rate constant of excited-state Ru(II) complexes by dialkyl sulfides and 4-nitrothioanisol are rather similar.[99] As shown in Figure 11, only photocatalysts with P(O)$(OEt)_2$ substituents in positions 4 and 7 gave the sulfoxide more rapidly than **Ru-phen** and **Ru-(bpy)$_3$**. Complex **Ru-4,7(PPh)$_2$** with the phenylene spacer gave the best results though **Ru-4,7P$_2$** and **Ru-4P** belonging to the series **Ru-P** were almost as active as this compound. High efficiency of **Ru-4,7(PPh)$_2$** is in good agreement with its increased singlet oxygen quantum yield, though this correlation was not observed for all complexes studied. For instance, complexes **Ru-4,7P$_2$** and **Ru-4P** having a rather different capabilities in generation of $^1O_2$ gave very similar oxidation rates.

Next, we tested the performance of the most efficient photocatalysts for oxidation of other sulfides. In the oxidation of benzyl methyl sulfide, **Ru-4,7(PPh)$_2$** and **Ru-4,7P$_2$** were as efficient as **Ru-4P** and all were superior to **Ru-phen** complex (Figure S34). The oxidation of 4-chlorothioanisol in the presence of **Ru-4,7(PPh)$_2$**, **Ru-4,7P$_2$** or **Ru-4P** proceeded also faster than with **Ru-phen** (Figure S35).

More theoretical and experimental investigation are certainly required to get better understanding of **Ru-Pcat** photocatalytic properties. Nevertheless, at this point we can safely conclude that complexes **Ru-4,7(PPh)$_2$** and **Ru-4,7P$_2$** are among the best (in terms of selectivity and the oxidation rate) known photocatalysts so far reported for oxidation of

organic sulfides to sulfoxides.[95] Although the direct comparison of reaction TONs for our photocatalysts and those reported earlier is not possible since these values are dependent on the irradiation intensity and other experimental conditions, we evaluated the TON for the oxidation of 4-chlorophenyl methyl sulfide in our conditions. When the most active **Ru-4,7P$_2$** photocatalyst was used, the quantitative synthesis of sulfoxide was achieved with a TON of almost 100000, i. e., 100 times higher than reported for oxidation of more reactive methyl phenyl sulfide in the recent work focused on the photocatalyst optimisation.[95] 4-Methoxyphenyl methyl sulfoxide was prepared in 99% yield with TON of about 1 000 000 and TOF of about 16 000 h^{-1}.

It is worth noting that photocatalytic procedures for selective formation of sulfoxide from sulfide are still scarce and, in most of them, specific photocatalysts immobilized on solid supports are employed.[100-105] Recently the selective photooxidation of sulfides was performed in the presence of Rose Bengal,[106] riboflavin[95] or BODIPY[107] derivatives employing 0.2–2 mol% of photocatalysts. It was also demonstrated that Ir(III) complexes are efficient in this reaction but the reaction scope was limited to alkyl aryl sulfides and 2-hydroxy-4-methylphenyl phenyl sulfide.[23]

Thus, we can conclude that the complexes **Ru-Pcat** are promising photocatalysts for performing both redox and EnT photocatalytic reactions. Comparative studies of reactivities of **Ru-phen**, **Ru-4,7(PPh)$_2$** and **Ru-4,7-P$_2$** can also be useful in mechanistic investigations of photoreactions.

CONCLUSIONS

We report here the study of a series of Ru(II) polypyridyl complexes (**Ru-Pcat**) of $[Ru(phen)(bpy)_2]^{2+}$-type, which are kinetically stable and have valuable optical and redox properties for application in organic photocatalysis. In this series, the phen ligand is modified by electron-withdrawing substituents $P(O)(OEt)_2$ and $4\text{-}(EtO)_2(O)PC_6H_4$ in order to tune redox potentials and excited-state energies and also to get access to grafting capabilities and developing novel heterogenized photocatalysts.

Synthetic approaches were developed to prepare these complexes in good yields. All newly synthesized compounds exhibited high photostability and good solubility in many polar solvents including chlorinated hydrocarbons. The coordination mode of ditopic phen ligands was confirmed by single crystal X-ray analysis of representative complexes (**Ru-5P** and **Ru-4,7P$_2$**) Their kinetic inertness in acetonitrile solutions was shown by NMR studies. Optical,

electrochemical and spectroelectrochemical properties were systematically investigated to get insight into the influence of $P(O)(OEt)_2$ groups on the electronic structure of these complexes. Electrochemical measurements showed that the first reduction ground state potentials, vary from –1.60 to –1.23 V (*vs* Ag^+/Ag) because the incoming electron occupies the π* orbital on the phen ligand in contrast to the parent **Ru-phen** complex where the bpy ligand lends this MO. The modifications of phen ligand cause small shifts in the metal-to-ligand charge-transfer absorption energies; brightness of most complexes is comparable to that of non-substituted **Ru-phen** and commonly used **Ru-(bpy)$_3$** complex. In contrast, the maximum of emission band is sensitive to substituents reaching the far-red region for **Ru-3,8P$_2$**. Electronic structure of complexes **Ru-Pcat** were obtained by DFT calculations using B3LYP functional providing comparison of newly synthesized compounds and their previously reported analogues.

It was also demonstrated in studies on the sulfides oxidation by molecular oxygen that the photoredox-catalyzed reactions can be benefited by tuning the structure of the catalyst. An acceleration of aryl sulfides oxidation was observed when **Ru-(bpy)$_3$** photocatalyst was replaced by complexes **Ru-4P** and **Ru-4,7P$_2$**.

The introduction of phenylene linker between the heteroaromatic ring and the phosphonate substituent significantly influence redox properties of complexes **Ru-Pcat** rendering ligands weaker as electron acceptors. Advantage of photocatalysts with the phenylene linker is observed in the singlet oxygen generation. This renders the complexes **Ru-PPh** good photocatalysts for the oxidation of organic substrates by molecular oxygen as it was demonstrated in this work by investigating the oxidation of dialkyl sulfides.

It is worth to note that the complexes with directly attached phosphonate group (**Ru-P**) and those containing phenylene linkers (**Ru-PPh**) exhibit different reactivity in the reactions proceeding through energy transfer and photoinduced electron transfer, which could be useful in that they can be used in mechanistic studies of photoreactions.

Complexes **Ru-Pcat** are attractive candidates for studies of homogeneous photocatalytic reactions owing to their high solubility in many solvents, high brightness and variable redox potentials that might impact the rate and selectivity of photocatalytic reactions. They are also promising for the development of reusable photocatalytic system, which is a final goal of our on-going studies. Such systems can be obtained by immobilization of **Ru-Pcat** on solid support (metal oxides) or into liquid-phases (liquid-liquid phase separation in which water-soluble Ru(II) complexes are immobilized in aqueous phase). The wide use of Ru(II) complexes in photocatalysis inevitably poses the questions of their cost, toxicity and

future accessibility, which can be solved only by the preparation of reusable photocatalytic systems. The knowledge gathered in this work is an indispensable background in the design of such reusable photocatalytic systems.

EXPERIMENTAL SECTION

Synthesis. General information on materials, methods and synthesis of ligands and complexes **Ru-Pcat** is present in Supporting Information.

X-ray crystallography of Ru-5P and Ru-4,7P$_2$. Single crystals of **Ru-5P** and **Ru-4,7P$_2$** were obtained by slow diffusion of toluene in solutions of complexes in $CHCl_3$/MeOH (1:1) mixture at 4°. The measurements were made on a Bruker SMART APEX II diffractometer with a CCD area detector (graphite monochromator, Mo-Kα radiation, λ= 0.71073 Å, ω-scanning, $2\theta_{max}$ = 56º). The semi-empirical method SADABS was applied for the absorption correction.[108] The structure was solved by direct methods and refined by the full-matrix least-squares technique against F^2 with the anisotropic displacement parameters for all non-hydrogen atoms. All the hydrogen atoms in the complexes were placed geometrically and included in the structure factors calculation in the riding motion approximation. All the data reduction and further calculations were performed using the SAINT and SHELXTL-97.[109]

Crystallographic data and refinement details are presented in Table S2; the main geometrical parameters of the studied complexes are listed in Tables S3 and Figures 2 and 3. Full tables of atomic coordinates, bond lengths, and valence angles are deposited in the Cambridge Structural Database (CCDC 2151157 (**Ru-5P**) and 2159570 (**Ru-4,7P$_2$**)). The data can be obtained free of charge from the Cambridge Crystallographic Data Centre at www.ccdc.cam.ac.uk/data_request/cif.

Structural investigation in solution. All NMR spectra were registered with Bruker Avance-400 spectrometer in $CDCl_3$ or CD_3CN. 2D NMR spectra of **Ru-4P** were recorded on the Agilent 400-MR instrument. Chemical shifts are expressed in parts per million (ppm), referenced on the δ scale by using residual non-deuterated solvent signals as internal standard for ^{1}H and ^{13}C NMR spectroscopy and external phosphonic acid (H_3PO_4) for ^{31}P NMR spectroscopy. The coupling constants are expressed in units of frequency (Hz).

Electrochemical and spectroelectrochemical characterization. Acetonitrile (Acros Organics, extra-dry with molecular sieves, water < 0.005%) was degassed using a freeze-

pump-thaw procedure and used as is in a Glove Box under N_2. Tetra-*n*-butylammonium hexafluorophosphate was prepared, purified and dried using standard procedures.

Cyclic voltammetry and voltammetry with rotating disc electrodes (RDE) were recorded using a SP300 Bilogic potentiostat. Analytical studies were conducted under N_2 (glove box) in a standard three–electrodes electrochemical cell. Tetra-*n*-butylammonium hexafluorophoshate was used as supporting electrolytes (0.1 M). An automatic ohmic drop compensation procedure (biologic ZIR) was systematically performed when using cyclic voltammetry. Vitreous carbon (Ø = 3 mm) working electrodes (CH Instruments) were polished with 1 mm diamond paste before each recording. Voltamperometry with a rotating disk electrode (RDE) was carried out with a radiometer (CTV101 radiometer analytical) equipment at a rotation rate of 500 rad min^{-1} using a glassy carbon RDE tip (Ø= 3 mm).

Spectroelectrochemical measurements were carried out at room temperature under N_2 (glove box) in dedicated batch "thin layer" type of cells (0.5 or 1 mm optical path lengths, Pt mesh electrodes, ALS Co. Ltd.) using a biologic SP300 potentiostat coupled to a MCS 601 UV-NIR Zeiss spectrophotometer. The counter–electrode was a platinum wire isolated from the electrolytic solution through an ionic bridge. $Ag/AgNO_3$ (CH Instruments, 10^{-2} M + TBAP 10^{-1} M in CH_3CN) was used as a reference electrode. Ferrocene was ultimately used as an internal reference. Measurements were carried out upon scanning the working electrode potential at 20 mV s^{-1} between the open circuit potential and a chosen final potential followed by microelectrolysis (1–5 min) at this potential.

Photophysical measurements. UV–vis spectra were recorded in solutions using a PerkinElmer Lambda 900 UV/VIS/NIR Spectrometer (1 cm path length quartz cell). Emission spectra were measured using a PerkinElmer LS 55 Luminescence Spectrometer. Emission quantum yields of all compounds were measured relative to the **Ru-(bpy)$_3$** in acetonitrile (Φ_{em} = 0.095) [64] and calculated using a standard procedure.[110]

Singlet oxygen generation quantum yields measurements were performed according to the literature.[111] To a solution of the $^1O_2$ trap, 1,9-dimethylanthracene (DMA), with an optical density of around 1.4 in air-saturated MeCN corresponding Ru(II) complex was added in a quartz cuvette, and its absorbance was adjusted to around 0.1 at the wavelength of irradiation. The solution in the cuvette was irradiated with 488 nm laser (Melles Griot 43 series i laser, 543R-AP-AO1) at a constant power density of 10 mW cm^{-2}. The absorption spectra of the solutions were measured every 30 s. The slope of plots of absorbance of DMA at 376 nm *vs* irradiation time for each photosensitizer was calculated.

Singlet oxygen quantum yields were calculated based on the equation:

$$\Phi_{\Delta} = \Phi_{\Delta}^{ref} \times \frac{k}{k_{ref}} \times \frac{I_{abs}^{ref}}{I_{abs}}$$

where Φ_{Δ} is the singlet oxygen quantum yield; the superscript ref stands for **Ru-(bpy)$_3$** (0.57 in acetonitrile)[65]; k is the slope of the curves of DMA absorption (376 nm) change vs. irradiation time; I_{abs} represents the absorption correction factor which is given by $I = 1–10^{–OD}$ (OD is the optical density at 488 nm).

Photocatalytic oxidation of sulfides. Standard 0.01 M solutions of **Ru-(bpy)$_3$**, **Ru-phen** and **Ru-Pcat** were prepared dissolving 0.05 mmol Ru(II) complexes in an acetonitrile/water (10:1 v/v) solvent mixture in 5 ml volumetric flasks.

General procedure. A glass vial equipped with a magnetic stir bar was charged with 1 mmol of sulfide (see Scheme 3) and calculated amount of standard solution of the photocatalyst. Then a mixture of MeCN/water (10:1 v/v) was added to obtain a solution of reagents in 2 mL of the solvent mixture. The reaction was irradiated with blue LED (30 W) for 4–6 h while gently bubbling oxygen. When the reaction was complete, the mixture was diluted with 7 mL of water and extracted with methylene chloride (3×5 mL). The combined extracts were dried over sodium sulfate and evaporated under reduced pressure at room temperature. The yield and purity of the products were determined by ^{1}H NMR using toluene as an internal standard.

Dialkyl sulfides were oxidized using 0.005 mol% of photocatalysts and the oxidation of aryl sulfides was performed in the presence of 0.05 mol% of photocatalysts as shown in Scheme 2. This catalysts loading was also used in kinetic studies (Figures 10, 11, S34 and S35) which were performed by using the same procedure. The reactions were periodically monitored by NMR spectroscopy after withdrawing aliquot samples.

ASSOCIATED CONTENT

Supporting Information

The supporting Information is available free of charge on the RSC Publications website at DOI: HR-ESI mass spectra, UV–vis spectra, NMR spectra for synthesized compounds; additional data on X-ray structures, electrochemistry, photocatalysis and DFT calculations.

Author contributions

J. M., A. Yu. M. and A. S. A. performed the synthesis of **P** ligands and **Ru-P** complexes. I. S. Z. prepared **PPh** ligands. G. V. M. optimized the synthesis of **PPh** ligands and **Ru-P** complexes, developed synthetic approaches to **Ru-PPh** complexes. M. A. F. performed photophysical characterization of all complexes and writing of the original draft of this article section. A. D. A. participated in characterization (NMR and mass spectroscopy) of newly synthesized compounds. V. A. R. performed specific NMR experiments allowing for the signal assignment in the spectra of **Ru-4P**. S. E. N. was responsible for single crystal X-ray characterization. C. B. performed electrochemical and spectroelectrochemical characterization of Ru complexes and writing of the original draft of this article section. A. V. C. performed DFT calculations. A. B.-L. studied photocatalytic properties of **Ru-Pcat** complexes. I. P. B. was responsible for data analysis, manuscript editing and funding acquisition. L. B. participated in manuscript editing. A. B.-L. and A. S. A. were responsible for the project conceptualization, supervision, data analysis, writing of article and funding acquisition.

ACKNOWLEDGMENTS

The authors thanks Prof. K. A. Lyssenko, Dr. Y. Bretonnière and Dr. S. Denis-Quanquin for help and useful discussions. This work was supported by the Russian Science Foundation (grant no. 20-73-00103). It was accomplished in the frame of the collaborative agreement between ENS de Lyon and Lomonosov Moscow State University (2012-2021). The 2D NMR spectra were recorded on the Agilent 400-MR instrument purchased by the MSU Development Program.

REFERENCES

1. Q. Zhao, F. Li and C. Huang, *Chem. Soc. Rev.*, 2010, **39**, 3007–3030.
2. F. Bella, C. Gerbaldi, C. Barolo and M. Grätzel, *Chem. Soc. Rev.*, 2015, **44**, 3431–3473.
3. D. L. Ashford, M. K. Gish, A. K. Vannucci, M. K. Brennaman, J. L. Templeton, J. M. Papanikolas and T. J. Meyer, *Chem. Rev.*, 2015, **115**, 13006–13049.
4. P. Alreja and N. Kaur, *RSC Advances*, 2016, **6**, 23169–23217.
5. N. Elgrishi, M. B. Chambers, X. Wang and M. Fontecave, *Chem. Soc. Rev.*, 2017, **46**, 761–796.

6. T. J. Meyer, M. V. Sheridan and B. D. Sherman, *Chem. Soc. Rev.*, 2017, **46**, 6148–6169.

7. A. A. Ghogare and A. Greer, *Chem. Rev.*, 2016, **116**, 9994–10034.

8. D. M. Schultz and T. P. Yoon, *Science*, 2014, **343**, 1239176.

9. J. M. R. Narayanam and C. R. J. Stephenson, *Chem. Soc. Rev.*, 2011, **40**, 102–113.

10. C. K. Prier, D. A. Rankic and D. W. C. MacMillan, *Chem. Rev.*, 2013, **113**, 5322–5363.

11. C. P. Anderson, D. J. Salmon, T. J. Meyer and R. C. Young, *J. Am. Chem. Soc.*, 1977, **99**, 1980–1982.

12. T.-J. J. Kinnunen, M. Haukka, M. Nousiainen, A. Patrikka and T. A. Pakkanen, *J. Chem. Soc., Dalton Trans.*, 2001, 2649–2654.

13. P. A. Mabrouk and M. S. Wrighton, *Inorg. Chem.*, 1986, **25**, 526–531.

14. K. R. Bargawi, A. Llobet and T. J. Meyer, *J. Am. Chem. Soc.*, 1988, **110**, 7751–7759.

15. A. E. Curtright and J. K. McCusker, *J. Phys. Chem. A*, 1999, **103**, 7032–7041.

16. X. Xiao, J. Sakamoto, M. Tanabe, S. Yamazaki, S. Yamabe and T. Matsumura-Inoue. *J. Electroanal. Chem.*, 2002, **527**, 33–40.

17. N. A. F. Al-Rawashdeh, S. Chatterjee, J. A. Krause and W. B. Connick, *Inorg. Chem.*, 2014, **53**, 294–307.

18. S. S. Bhat, A. S. Kumbhar, P. Lönnecke and E. Hey-Hawkins, *Inorg. Chem.*, 2010, **49**, 4843–4853.

19. P. J. DeLaive, J. T. Lee, H. W. Sprintschnik, H. Abruna, T. J. Meyer and D. G. Whitten, *J. Am. Chem. Soc.*, 1977, **99**, 7094–7097.

20. T. Rajendran, P. Thanasekaran, S. Rajagopal, G. A. Gnanaraj, C. Srinivasan, P. Ramamurthy, B. Venkatachalapathy, B. Manimaran and K.-L. Lu, *Phys. Chem. Chem. Phys.*, 2001, **3**, 2063–2069.

21. E. Deponti and M. Natali, *Dalton Trans.*, 2016, **45**, 9136–9147.

22. H. Shalan, A. Colbert, T. T. Nguyen, M. Kato and L. Cheruzel, *Inorg. Chem.*, 2017, **56**, 6558–6564.

23. L.-P. Li and B.-H. Ye, *Inorg. Chem.*, 2019, **58**, 7775–7784.

24. S. DiLuzio, T. U. Connell, V. Mdluli, J. F. Kowalewski and S. Bernhard, *J. Am. Chem. Soc.*, 2022, **144**, 1431–1444.

25. M. Liras, M. Pintado-Sierra, M. Iglesias and F. Sánchez, *J. Mat. Chem. A*, 2016, **4**, 17274–17278.

26. C. Queffélec, M. Petit, P. Janvier, D. A. Knight and B. Bujoli, *Chem. Rev.*, 2012, **112**, 3777−3807.

27. G. Guerrero, J. G. Alauzun, M. Granier, D. Laurencin and P. H. Mutin, *Dalton Trans.*, 2013, **42**, 12569–12585.

28. H. Zabri, I. Gillaizeau, C. A. Bignozzi, S. Caramori, M.-F. Charlot, J. Cano-Boquera and F. Odobel, *Inorg. Chem.*, 2003, **42**, 6655–6666.

29. P. Wang, C. Klein, J.-E. Moser, R. Humphry-Baker, N.-L. Cevey-Ha, R. Charvet, P. Comte, S. M. Zakeeruddin and M. Grätzel, *J. Phys. Chem. B*, 2004, **108**, 17553–17559.

30. M. R. Norris, J. J. Concepcion, C. R. K. Glasson, Z. Fang, A. M. Lapides, D. L. Ashford, J. L. Templeton and T. J. Meyer, *Inorg. Chem.*, 2013, **52**, 12492–12501.

31. K. Neuthe, F. Bittner, F. Stiemke, B. Ziem, J. Du, M. Zellner, M. Wark, T. Schubert and R. Haag, *Dyes Pigm.*, 2014, **104**, 24–33.

32. D. L. Ashford, M. K. Brennaman, R. J. Brown, S. Keinan, J. J. Concepcion, J. M. Papanikolas, J. L. Templeton and T. J. Meyer, *Inorg. Chem.*, 2015, **54**, 460–469.

33. M. M. Raber, M. D. Brady, L. Troian-Gautier, J. C. Dickenson, S. L. Marquard, J. T. Hyde, S. J. Lopez, G. J. Meyer, T. J. Meyer and D. P. Harrison, *ACS Appl. Mater. Interfaces*, 2018, **10**, 22821–22833.

34. M. D. Brady, L. Troian-Gautier, R. N. Sampaio, T. C. Motley and G. J. Meyer, *ACS Appl. Mater. Interfaces*, 2018, **10**, 31312–31323.

35. S. L. Esarey and B. M. Bartlett, *Langmuir*, 2018, **34**, 4535–4547.

36. P. Farràs, C. Di Giovanni, J. N. Clifford, E. Palomares and A. Llobet, *Coord. Chem. Rev.*, 2015, **304**–**305**, 202–208.

37. S. Reischauer, V. Strauss and B. Pieber, *ACS Catal.*, 2020, **10**, 13269–13274.

38. S. Reischauer and B. Pieber, *ChemPhotoChem*, 2021, **5**, 716–720.

39. A.-C. Laemmel, J.-P. Collin and J.-P. Sauvage, *Eur. J. Inorg. Chem.*, 1999, 383–386.

40. A. Yu. Mitrofanov, PhD thesis, Université de Bourgogne and Lomonosov Moscow state university, Dijon, France and Moscow, Russia, 2015.

41. S. Amthor, P. Keil, D. Nauroozi, D. Perleth and S. Rau, *Eur. J. Inorg. Chem.*, 2021, 4790–4798.

42. A. Mitrofanov, A. B. Lemeune, C. Stern, R. Guilard, N. Gulyukina and I. Beletskaya, *Synthesis*, 2012, **44**, 3805–3810.

43. A. Mitrofanov, S. Brandes, F. Herbst, S. Rigolet, A. Bessmertnykh-Lemeune and I. Beletskaya, *J. Mat. Chem. A*, 2017, **5**, 12216–12235.

44. B.-H. Ye, L.-N. Ji, F. Xue and T. C. W. Mak, *Transition Met. Chem.*, 1999, **24**, 8–12.

45. B.-H. Ye, X.-M. Chen, T.-X. Zeng and L.-N. Ji, *Inorg. Chim. Acta*, 1995, **240**, 5–11.

46. D. S. Eggleston, K. A. Goldsby, D. J. Hodgson and T. J. Meyer, *Inorg. Chem.*, 1985, **24**, 4573–4580.

47. D. P. Rillema, D. S. Jones, C. Woods and H. A. Levy, *Inorg. Chem.*, 1992, **31**, 2935–2938.

48. C. M. Elliott and E. Hershenhart, *J. Am. Chem. Soc.*, 1982, **104**, 7519–7526.

49. V. V. Pavlishchuk and A. W. Addison, *Inorg. Chim. Acta*, 2000, **298**, 97–102.

50. A. Juris, V. Balzani, F. Barigelletti, S. Campagna, P. Belser and A. von Zelewsky, *Coord. Chem. Rev.*, 1988, **84**, 85–277.

51. M. Montalti, S. Wadhwa, W. Y. Kim, R. A. Kipp and R. H. Schmehl, *Inorg. Chem.*, 2000, **39**, 76–84.

52. P. S. Braterman, J.-I. Song and R. D. Peacock, *Spectrochim. Acta, Part A*, 1992, **48**, 899–903.

53. N. Yoshikawa, S. Yamabe, S. Sakaki, N. Kanehisa, T. Inoue and H. Takashima, *J. Mol. Struct.*, 2015, **1094**, 98–108.

54. T. Véry, D. Ambrosek, M. Otsuka, C. Gourlaouen, X. Assfeld, A. Monari and C. Daniel, *Chem. – Eur. J.*, 2014, **20**, 12901–12909.

55. V. Balzani, A. Juris, M. Venturi, S. Campagna and S. Serroni, *Chem. Rev.*, 1996, **96**, 759–834.

56. A. Ghosh, B. Ganguly and A. Das, *Inorg. Chem.*, 2007, **46**, 9912–9918.

57. C. T. Lin, W. Boettcher, M. Chou, C. Creutz and N. Sutin, *J. Am. Chem. Soc.*, 1976, **98**, 6536–6544.

58. P. C. Alford, M. J. Cook, A. P. Lewis, G. S. G. McAuliffe, V. Skarda, A. J. Thomson, J. L. Glasper and D. J. Robbins, *J. Chem. Soc., Perkin Trans. 2*, 1985, 705–709.

59. H. Suzuki, T. Kanbara and T. Yamamoto, *Inorg. Chim. Acta*, 2004, **357**, 4335–4340.

60. A. M. Pyle, J. P. Rehmann, R. Meshoyrer, C. V. Kumar, N. J. Turro and J. K. Barton, *J. Am. Chem. Soc.*, 1989, **111**, 3051–3058.

61. J. K. Barton, J. K. US Pat., 5157032, 1992.

62. K. Mori, M. Kawashima, K. Kagohara and H. Yamashita, *J. Phys. Chem. C*, 2008, **112**, 19449–19455.

63. H. Ishida, S. Tobita, Y. Hasegawa, R. Katoh and K. Nozaki, *Coord. Chem. Rev.*, 2010, **254**, 2449–2458.

64. A. A. Abdel-Shafi, P. D. Beer, R. J. Mortimer and F. Wilkinson, *J. Phys. Chem. A*, 2000, **104**, 192–202.

65. J. Al-Nu'airat, I. Oluwoye, N. Zeinali, M. Altarawneh and B. Z. Dlugogorski, *Chem. Rec.*, 2021, **21**, 315–342.

66. A. A. Granovsky, *Firefly version 8*, http://classic.chem.msu.su/gran/firefly/index.html.

67. M. W. Schmidt, K. K. Baldridge, J. A. Boatz, S. T. Elbert, M. S. Gordon, J. H. Jensen, S. Koseki, N. Matsunaga, K. A. Nguyen, S. Su, T. L. Windus, M. Dupuis and J. A. Montgomery, *J. Comput. Chem.*, 1993, **14**, 1347–1363.

68. M. Dolg, H. Stoll, H. Preuss and R. M. Pitzer, *J. Phys. Chem.*, 1993, **97**, 5852–5859.

69. D. F. Zigler, Z. A. Morseth, L. Wang, D. L. Ashford, M. K. Brennaman, E. M. Grumstrup, E. C. Brigham, M. K. Gish, R. J. Dillon, L. Alibabaei, G. J. Meyer, T. J. Meyer and J. M. Papanikolas, *J. Am. Chem. Soc.*, 2016, **138**, 4426–4438.

70. D. F. Zigler, Z. A. Morseth, L. Wang, D. L. Ashford, M. K. Brennaman, E. M. Grumstrup, E. C. Brigham, M. K. Gish, R. J. Dillon, L. Alibabaei, G. J. Meyer, T. J. Meyer and J. M. Papanikolas, J. Am. Chem. Soc., 2016, 138, 4426–4438.

71. F. Alary, J. L. Heully, L. Bijeire and P. Vicendo, Inorg. Chem., 2007, 46, 3154–3165.

72. A. Dreuw and M. Head-Gordon, Chem. Rev., 2005, 105, 4009–4037.

73. S. Grimme and M. Parac, ChemPhysChem, 2003, 4, 292–295.

74. A. Dreuw and M. Wormit, Wiley Interdiscip. Rev.: Comput. Mol. Sci., 2015, 5, 82–95.

75. E. L. Clennan, *Acc. Chem. Res.*, 2001, **34**, 875–884.

76. J. W. Tucker and C. R. J. Stephenson, *J. Org. Chem.*, 2012, **77**, 1617–1622.

77. V. Balzani, F. Bolletta, M. T. Gandolfi and M. Maestri, In *Organic chemistry and theory. Topics in current chemistry* Springer Berlin Heidelberg: Berlin, Heidelberg, 1978, pp 1–64.

78. S. Miller, *Environ. Sci. Technol.*, 1990, **24**, 1286–1289.

79. K. A. Stingl and S. B. Tsogoeva, *Tetrahedron: Asymmetry*, 2010, **21**, 1055–1074.

80. Y. Liu, A. J. Howarth, J. T. Hupp and O. K. Farha, *Angew. Chem., Int. Ed.*, 2015, **54**, 9001–9005.

81. X. Lang, W. Hao, W. R. Leow, S. Li, J. Zhao and X. Chen, *Chem. Sci.*, 2015, **6**, 5000–5005.

82. G. Sipos, E. E. Drinkel and R. Dorta, *Chem. Soc. Rev.*, 2015, **44**, 3834–3860.

83. G. Laudadio, N. J. W. Straathof, M. D. Lanting, B. Knoops, V. Hessel and T. Noël, *Green. Chem.*, 2017, **19**, 4061–4066.

84. *Sulfur Chemistry*, Jiang, X., ed.; Springer, Berlin, 2019.

85. E. Baciocchi, C. Rol, E. Scamosci and G. V. Sebastiani, *J. Org. Chem.*, 1991, **56**, 5498–5502.

86. E. Baciocchi, C. Crescenzi and O. Lanzalunga, *Tetrahedron*, 1997, **53**, 4469–4478.

87. E. Baciocchi, T. Del Giacco, M. F. Gerini and O. Lanzalunga, *Org. Lett.*, 2006, **8**, 641–644.

88. J. Legros, J. R. Dehli and C. Bolm, *Adv. Synth. Catal.*, 2005, **347**, 19–31.

89. S. Caron, R. W. Dugger, S. G. Ruggeri, J. A. Ragan and D. H. B. Ripin, *Chem. Rev.*, 2006, **106**, 2943–2989.

90. E. Baciocchi, T. D. Giacco, F. Elisei, M. F. Gerini, M. Guerra, A. Lapi and P. Liberali, *J. Am. Chem. Soc.*, 2003, **125**, 16444–16454.

91. S. M. Bonesi, I. Manet, M. Freccero, M. Fagnoni and A. Albini, *Chem. – Eur. J.*, 2006, **12**, 4844–4857.

92. S. M. Bonesi, M. Fagnoni and A. Albini, *Eur. J. Org. Chem.*, 2008, 2612–2620.

93. H. Yokoi, A. Hatta, K. Ishiguro and Y. Sawaki, *J. Am. Chem. Soc.*, 1998, **120**, 12728–12733.

94. E. Baciocchi, T. Del Giacco, F. Elisei and A. Lapi, *J. Org. Chem.*, 2006, **71**, 853–860.

95. T. Neveselý, E. Svobodová, J. Chudoba, M. Sikorski and R. Cibulka, *Adv. Synth. Catal.*, 2016, **358**, 1654–1663.

96. G. Bianchini, A. Scarso, G. L. Sorella and G. Strukul, *Chem. Commun.*, 2012, **48**, 12082–12084.

97. S. M. Bonesi, M. Mella, N. d'Alessandro, G. G. Aloisi, M. Vanossi and A. Albini, *J. Org. Chem.*, 1998, **63**, 9946–9955.

98. E. L. Clennan, W. Zhou and J. Chan, *J. Org. Chem.*, 2002, **67**, 9368–9378.

99. E. Rajkumar and S. Rajagopal, *Photochem. Photobiol. Sci.*, 2008, **7**, 1407–1414.

100. J.-M. Zen, S.-L. Liou, A. S. Kumar and M.-S. Hsia, *Angew. Chem., Int. Ed.*, 2003, **42**, 577–579.

101. C. Wang, Z. Xie, K. E. deKrafft and W. Lin, *J. Am. Chem. Soc.*, 2011, **133**, 13445–13454.

102. H. Yang and H. Fei, *Dalton Trans.*, 2017, **46**, 2751–2755.

103. X. Zhang, X. Zhang, J. A. Johnson, Y.-S. Chen and J. Zhang, *J. Am. Chem. Soc.*, 2016, **138**, 8380–8383.

104. Z.-Y. Xu, Y. Luo, D.-W. Zhang, H. Wang, X.-W. Sun and Z.-T. Li, *Green. Chem.*, 2020, **22**, 136–143.

105. H.-P. Liang, Q. Chen and B.-H. Han, *ACS Catal.*, 2018, **8**, 5313–5322.

106. X. Gu, X. Li, Y. Chai, Q. Yang, P. Li and Y. Yao, *Green. Chem.*, 2013, **15**, 357–361.

107. W. Li, Z. Xie and X. Jing, *Catal. Commun.*, 2011, **16**, 94–97.

108. G. Sheldrick, *Bruker AXS Inc.*, Madison, USA, 1997.

109. *Bruker SAINT: Area-Detector Integration Sofware, 2012*, Madison, Wisconsin, USA, 2012.

110. M. Levitus, *Methods Appl. Fluoresc.*, 2020, **8**, 033001.

111. L. Gou, C. N. Coretsopoulos and A. B. Scranton, *J. Polym. Sci., Part A: Polym. Chem.*, 2004, **42**, 1285–1292.

111. L. Gou, C. N. Coretsopoulos and A. B. Scranton, *Journal of Polymer Science Part A: Polymer Chemistry*, 2004, **42**, 1285-1292.